

Fluid–Rock Interaction in the Miocene, Post-Caldera, Tejeda Intrusive Complex, Gran Canaria (Canary Islands): Insights from Mineralogy, and O- and H-Isotope Geochemistry

ELEANOR DONOGHUE^{1*}, VALENTIN R. TROLL² AND CHRIS HARRIS³

¹DEPARTMENT OF GEOLOGY, UNIVERSITY OF DUBLIN, TRINITY COLLEGE, DUBLIN 2, IRELAND

²DEPARTMENT OF EARTH SCIENCES, UPPSALA UNIVERSITY, VILLAVÄGEN 16, SE-752 36 UPPSALA, SWEDEN

³DEPARTMENT OF GEOLOGICAL SCIENCES, UNIVERSITY OF CAPE TOWN, RONDEBOSCH 7701, SOUTH AFRICA

RECEIVED DECEMBER 2, 2008; ACCEPTED AUGUST 12, 2010

The intra-caldera volcanoclastic deposits of the Miocene Tejeda caldera on Gran Canaria host an ~12 km diameter intrusive complex comprising a peralkaline, trachytic to phonolitic cone sheet swarm surrounding a central core of hypabyssal syenite stocks. Both intrusive rock types display textural and mineralogical features indicative of secondary fluid–rock interaction, including (1) deuteric mineral phases (e.g. aegirine, alkali-amphibole, analcime), (2) turbid alkali feldspars, and (3) hydrothermal mineral phases (phyllosilicates, Fe–Ti oxides, Mn-oxides, and quartz). Altered cone sheets have whole-rock $\delta^{18}\text{O}$ values ranging from 0.1 to 10.0‰ (n = 22), and whole-rock δD values between –62 and –149‰ (n = 28). Three altered syenite samples have whole-rock $\delta^{18}\text{O}$ values of 2.5, 1.5, and 0.9‰, and corresponding δD values of –91, –99, and –121‰. The H_2O concentrations of the altered cone sheets range from 0.4 to 0.8 wt % (n = 28), and the altered syenites have H_2O concentrations of 0.5, 0.5, and 0.6 wt %, respectively. The majority of altered samples are depleted in ^{18}O relative to the typical $\delta^{18}\text{O}$ range for unaltered trachytes and syenites ($\delta^{18}\text{O} = 6–8‰$), indicative of interaction with local meteoric water ($\delta^{18}\text{O}$ c. –8‰) at temperatures $\geq 150^\circ\text{C}$. Only one cone sheet sample appears petrographically unaltered and has a typical ‘igneous’ isotopic composition ($\delta^{18}\text{O} = 7.1‰$, $\delta\text{D} = -48‰$) and a relatively high H_2O concentration (2.2 wt %). A weak correlation ($r = 0.55$) between δD and H_2O is observed in the cone sheets, reflecting the combined effects of magmatic H_2O exsolution, and subsequent deuteric and

hydrothermal alteration. No systematic variation in $\delta^{18}\text{O}$ or δD was detected across the cone sheet swarm, most likely reflecting overprinting of isotopic compositions during successive intrusive events. However, the highest $\delta^{18}\text{O}$ values (8.2–10.0‰) occur in clay-bearing cone sheets from the central part of the intrusive complex, suggesting enhanced infiltration of relatively cool meteoric water in this area. Overall, at least three phases of fluid–rock interaction can be distinguished: (1) deuteric alteration (c. 300–500°C) by late magmatic fluids expelled from a solidifying crystal mush; (2) hydrothermal alteration ($\geq 150–300^\circ\text{C}$) by meteoric water during the final stages of crystallization and/or immediately following solidification of the intrusive complex; (3) retrograde alteration related to the influx of relatively cool ($\leq 150^\circ\text{C}$) meteoric waters.

KEY WORDS: cone sheets; Gran Canaria; hydrothermal alteration; intrusive complexes; stable isotopes; Tejeda caldera

INTRODUCTION

Plutonic and hypabyssal intrusive rocks typically form the subvolcanic cores, or ‘root zones’, of overlying volcanic centres. These intrusive rocks may take various geometric forms, including sills, central intrusions, ring dykes, swarms of sub-vertical sub-parallel dykes, sub-vertical

*Corresponding author. E-mail: donoghue@tcd.ie

radial dykes, or inward-dipping concentric intrusions with a common focus (cone sheets), and may become exposed after uplift and subsequent erosion of overlying formations (e.g. McBirney, 1993). During emplacement and cooling, crystals that grow in the intrusive bodies may interact with magmatic–hydrothermal (deuteric) volatiles (e.g. H₂O, HCl, H₂, CO₂, CH₄, SO₂) that have exsolved during the final stages of crystallization (e.g. Burnham & Ohmoto, 1980; Burnham, 1997). If the intrusions are emplaced into relatively permeable country rocks at shallow levels (~2–6 km), they may also be susceptible to the influx of heated meteoric groundwaters during and after solidification (e.g. Taylor, 1968, 1977; Taylor & Forester, 1970; Criss & Taylor, 1986). Such fluid–rock interactions often result in distinctive textural, mineralogical, and isotopic (particularly O and H) changes within the intrusive bodies and their surrounding country rocks, reflecting the characteristic fluid sources, compositions, temperatures, and flow paths (e.g. Taylor, 1997).

Petrological and stable isotope studies have been conducted on numerous epizonal intrusive complexes affected by fluid–rock interaction. Among the most well-documented examples are the Tertiary intrusive complexes of the Inner Hebrides, NW Scotland (e.g. Forester & Taylor, 1976, 1977; Ferry, 1985*a*, 1985*b*), and the layered mafic intrusions of East Greenland (e.g. Taylor & Epstein, 1963; Fehlhaber & Bird, 1991; Brandriss *et al.*, 1995). Most notably, the above studies all highlighted the occurrence of intrusive rocks with abnormally low $\delta^{18}\text{O}$ values (down to -7%) compared with ‘normal’ igneous rocks ($\delta^{18}\text{O} = 6\text{--}8\%$; e.g. Taylor, 1968), providing unequivocal evidence for oxygen isotope exchange with heated, ^{18}O -depleted meteoric waters. Hydrothermal alteration is largely thought to take place following solidification, when the intrusive rocks are cool enough to fracture and allow infiltration of surrounding hydrothermal fluids (e.g. Criss & Taylor, 1986; Larson & Taylor, 1986*a*).

In the Canary Archipelago, hydrothermal and metamorphic processes involving meteoric water have been reported for the intrusive rocks of Fuerteventura, Tenerife, La Gomera, and La Palma (e.g. Javoy *et al.*, 1986; Schiffman & Staudigel, 1994, 1995; Wolff *et al.*, 2000; Rodríguez Losada & Martínez Frias, 2004; Holloway *et al.*, 2008). On Gran Canaria, epithermal alteration associated with the marginal volcanic rocks of the Miocene Tejeda caldera has been described by Schmincke (1998), Pérez Torrado *et al.* (2004), Cabrera Santana *et al.* (2006) and Donoghue *et al.* (2008), providing evidence for the development of a large-scale, intrusion-related, meteoric–hydrothermal system during caldera volcanism. As yet, however, the hydrothermal system and associated alteration of the post-caldera Tejeda Intrusive Complex has not been examined in detail. In this study, we describe (1) the mineralogical and isotopic changes brought

about by fluid–rock interaction in the Tejeda Intrusive Complex, (2) the main fluid source(s) and flow pathways, (3) the thermal evolution of the hydrothermal system, (4) the influence of multiple intrusions and caldera resurgence on the intensity of alteration, and the corresponding isotopic composition of the intrusive rocks, and (5) the spatial and temporal relationship between the epithermal and intrusive hydrothermal systems within the Tejeda caldera.

GEOLOGICAL SETTING

The Canary Archipelago is a NE–SW-trending alignment of seven volcanic ocean islands located 100–700 km off the NW African coast (Fig. 1), believed to originate from a hot-spot beneath the passive margin of the African continent (e.g. Hoernle & Schmincke, 1993; Carracedo *et al.*, 1998). Gran Canaria (28°00'N, 15°35'W), one of the central islands of the archipelago, comprises a Miocene basaltic shield (~15–14 Ma), overlain by an up to 1000 m thick succession of felsic extrusive rocks, which form the outflow facies of the 20 km diameter, multiply reactivated Tejeda caldera in the centre of the island (e.g. Schmincke, 1982; Schirnack *et al.*, 1999; Troll *et al.*, 2002). The felsic eruptive rocks comprise a lower succession of ~20 subalkaline to peralkaline trachyte and rhyolite ignimbrites (Mogán Group, 14–13.3 Ma), and an overlying series of ~20 trachy-phonolite ignimbrites and lava flows (Fataga Group, 12.4–8.5 Ma) (e.g. van den Bogaard & Schmincke, 1998). A well-exposed outer caldera margin separates the extra-caldera shield lavas and overlying felsic ignimbrites from intra-caldera sediments, ignimbrites, and intrusive rocks (e.g. Schmincke, 1967). Correlation of intra-caldera ignimbrites with the extra-caldera ignimbrite succession suggests subsidence of the caldera basin of at least 1 km (Schmincke & Swanson, 1966; Schmincke, 1982; Troll *et al.*, 2002). Following Miocene volcanic activity, there was a major volcanic hiatus between ~8 and 5 Ma. Volcanic activity resumed with the eruption of lavas, tuffs and breccias of the Pliocene Roque Nublo Group (5–3.5 Ma), followed by a major phase of dominantly nephelinite volcanism (Post-Roque Nublo Group; <3 Ma) (e.g. van den Bogaard & Schmincke, 1998).

THE TEJEDA INTRUSIVE COMPLEX

The ~12 km diameter Tejeda Intrusive Complex (12.3–7.3 Ma; Schirnack *et al.*, 1999) is centred in the western part of the Tejeda caldera, and comprises a central core of hypabyssal syenite stocks, surrounded by three concentric zones of both high- and low-density cone sheet intrusions: (1) a 2–3 km wide Annular Low Density Zone (ALDZ)

Gran Canaria

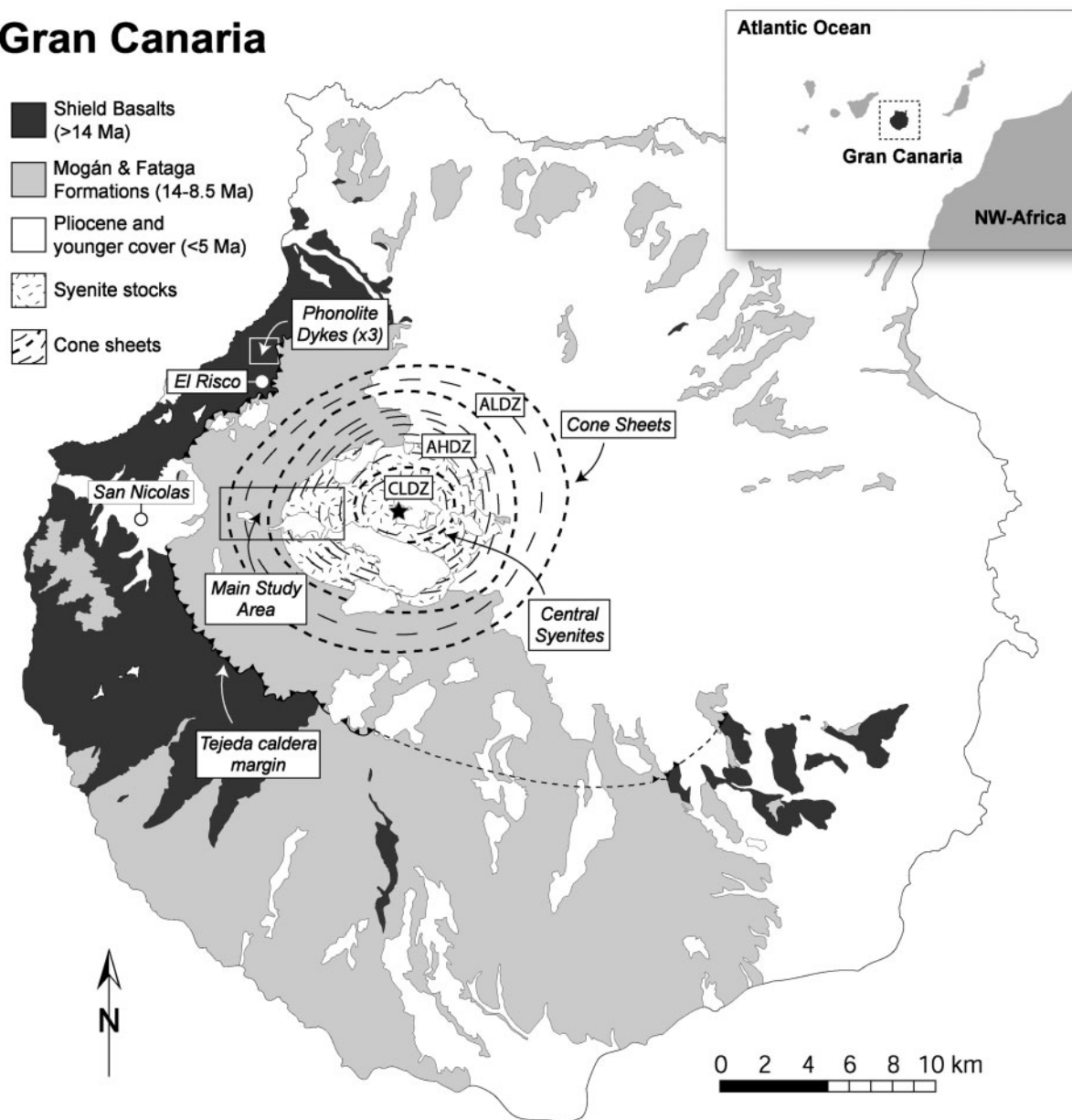


Fig. 1. Simplified geological map of Gran Canaria, showing the cone sheets and syenites of the Tejeda Intrusive Complex, the location of the main sample traverse, and the sample area for the three extra-caldera phonolite dykes. The cone sheet swarm is subdivided into three concentric zones: CLDZ, Central Low Density Zone; AHDZ, Annular High Density Zone; ALDZ, Annular Low Density Zone. Star marks central axis of radial symmetry (see Schmincke, 1998; Schirnack *et al.*, 1999).

containing <20% cone sheets; (2) a 2.5–4 km diameter Annular High Density Zone (AHDZ) with 50–100% cone sheets; (3) a 4 km diameter Central Low Density Zone (CLDZ) comprising intra-caldera breccias intruded by syenite stocks and <20% cone sheets (e.g. Hernan & Vález, 1980; Schmincke, 1998; Schirnack *et al.*, 1999; Figs 1–3). Whole-rock geochemical variations suggest that the trachytic–phonolitic cone sheet magmas originated by

fractional crystallization from less-evolved trachytic magmas, whereas the central syenites represent the crystalline residue of this process (Schirnack, 1996).

The exposed cone sheets and syenites intrude older intra-caldera trachy-phonolitic ignimbrites and lava flows, which are compositional equivalents of the extra-caldera Fataga Group (Schmincke, 1976; van den Bogaard & Schmincke, 1998). Several hundred metres of intra-caldera

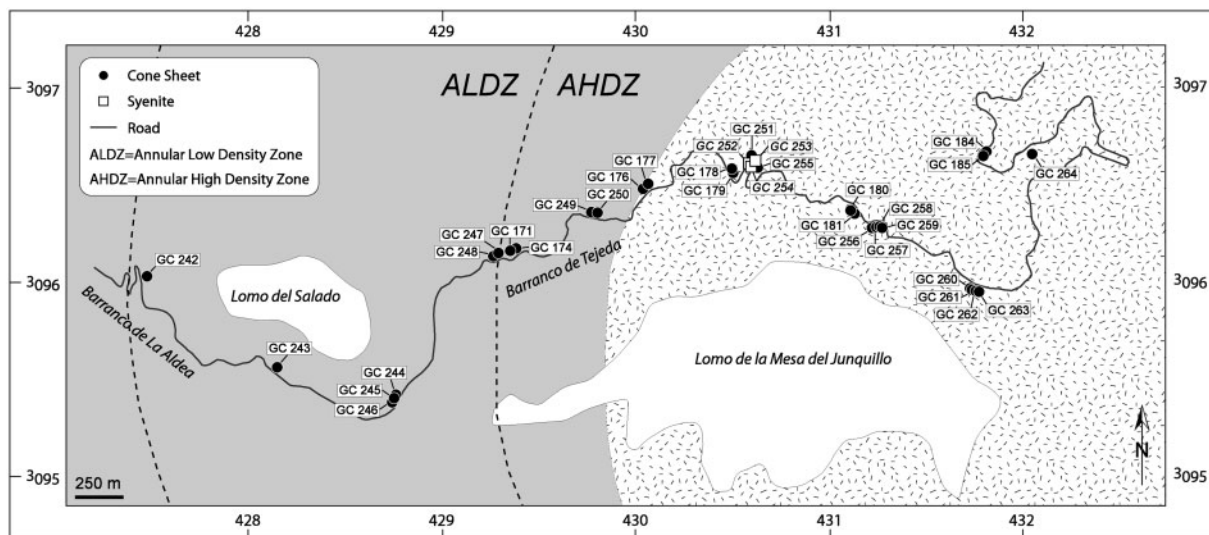


Fig. 2. Detailed map of the main study area, showing the sample localities. Lithological units shaded as in Fig. 1.

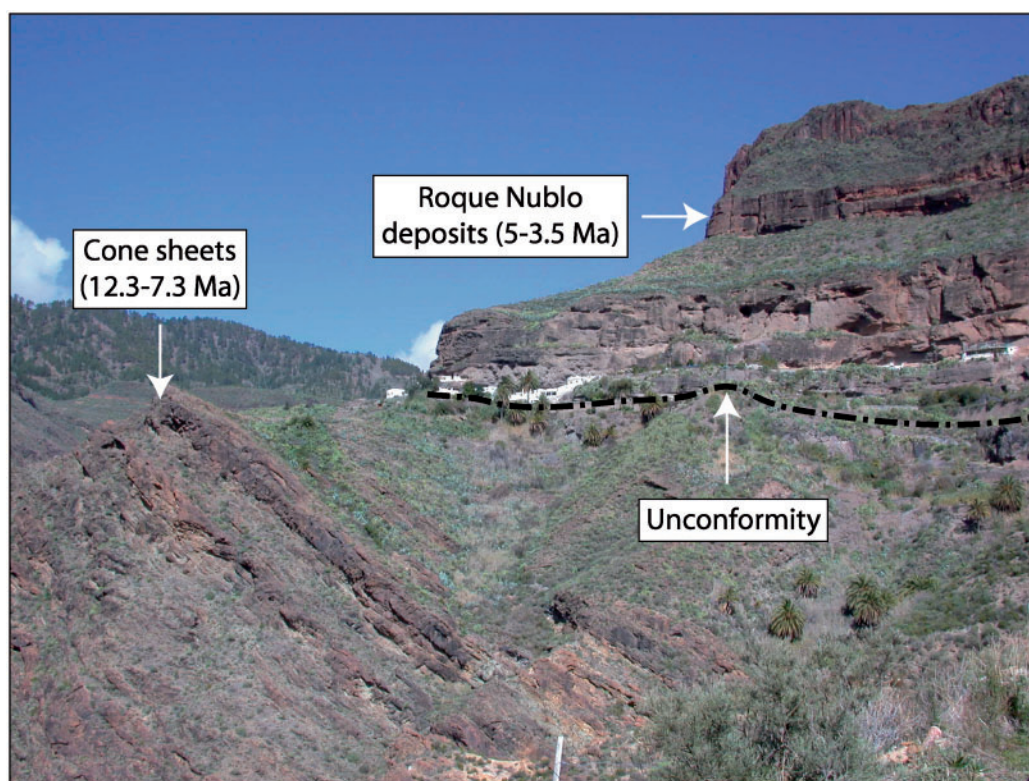


Fig. 3. View of the north face of Mesa de Junquillo [431000, 3095800] showing the unconformity between eastward-dipping cone sheets of the Miocene Tejada Intrusive Complex (lower left), and flat-lying lavas and breccias of the Pliocene Roque Nublo group (top right).

ignimbrites and lavas of the middle and lower Mogán formations are thought to form the host-rocks for the cone sheets below the present level of exposure. The 40° dipping cone sheets form a spectacular unconformity with the

flat-lying lavas and breccias of the Roque Nublo group (5–3.5 Ma; van den Bogaard & Schmincke, 1998) at Mesa de Junquillo (Fig. 3), representing a period of volcanic quiescence and deep erosion between ~8 and 5 Ma.

Intrusive activity was relatively intense (repose intervals of ~5–10 kyr between intrusions, compared with >50 kyr between eruptions), and persisted during periods of both volcanic activity and inactivity (Schirnick *et al.*, 1999). Two generations of cone sheets have been distinguished, representing a total of 500–1000 intrusive events. An older generation of porphyritic, alkali feldspar trachyte cone sheets (12.3–9.5 Ma) is preserved mainly in the outermost part of the ALDZ, whereas a younger generation of aphanitic, alkali feldspar trachytic to phonolitic cone sheets (9.7–7.3 Ma) dominates the AHDZ and CLDZ. The syenite stocks intruded the AHDZ at 12.3 and 9.88 Ma, and the CLDZ at 8.94 Ma. Together, the cone sheets and syenite stocks represent a bulk intrusive volume of >250 km³, and resulted in a calculated cumulative uplift of at least 2 km within the Tejeda caldera (Schirnick, 1996; Schirnick *et al.*, 1999).

To date, investigations into the hydrothermal alteration associated with the Tejeda Intrusive Complex have been limited. Schirnick (1996) noted that Fe–Ti oxides (magnetite and ilmenite) in the older generation cone sheets have been altered to hydroxides (leucocoxene), and that oxides in the central syenites display exsolution textures indicative of highly oxidizing conditions. Schirnick *et al.* (1999) reported that alkali-feldspars in the older generation cone sheets are pervasively altered, and have undergone sub-solidus exsolution to albite and orthoclase, whereas feldspars from the younger generation cone sheets are unaltered. Those workers therefore suggested that hydrothermal activity associated with the intrusive complex ended before 9.54 ± 0.03 Ma, the minimum age of the older cone sheet generation. Schmincke (1998) also noted that some of the trachyte cone sheets of the AHDZ display ‘characteristic ochre weathering colours’, and suggested that cone sheet alteration might represent a second pulse of hydrothermal activity that reached its peak during late Fataga time (i.e. separate to the marginal, late Mogán epithermal system described by, e.g. Donoghue *et al.*, 2008). However, Schmincke (1998) also noted that the lowermost formations of the Fataga group exposed in the direct vicinity of the caldera margin appear relatively unaltered compared with underlying upper Mogán ignimbrites, and suggested that alteration of the cone sheets may alternatively reflect inward ‘shrinking’ of a single Miocene hydrothermal system between late Mogán and Fataga times. Thus, the exact nature and timing of the intrusive hydrothermal system on Gran Canaria remains unresolved. This study provides new insight into the mineralogical and geochemical evolution of the hydrothermal system associated with the Tejeda Intrusive Complex, and sheds new light on its spatial and temporal relationship to the intense alteration of the volcanic rocks along the Tejeda caldera margin.

SAMPLING AREA AND FIELD OBSERVATIONS

The area selected for investigation lies along an ~8 km stretch of the GC-210 road, extending from the eastern end of Barranco de La Aldea [427444, 3096025; all grid references reported according to the WGS84 datum and UTM projection] to the central part of Barranco de Tejeda [432048, 3096577] (Fig. 2). The road section traverses both the ALDZ and AHDZ, which together account for over 70% of the exposed cone sheets of the intrusive complex (Schmincke, 1998; Schirnick *et al.*, 1999). The road section also cuts through the central syenite stocks in Barranco de Tejeda at [430568, 3096773] (Fig. 2), allowing the full range of intrusion types to be sampled. Deep erosion and almost continuous exposure of cone sheets of variable age and composition in this area (Schirnick *et al.*, 1999) facilitated a detailed west to east sample traverse from the margin to the central part of the cone sheet swarm, thereby allowing us to constrain any spatial and/or temporal variations in alteration intensity, style, and isotopic composition across the intrusive complex.

On an outcrop and hand-sample scale (Fig. 4a–d), the altered cone sheets are generally massive, and display ubiquitous Mn-oxide staining, veining or fluidal textures and dark grey–purple alteration colours. A number of cone sheets closer to the centre of the cone sheet swarm (e.g. GC185) are intensely friable, and display bright green and beige alteration colours (Fig. 4b and d). The intensity of alteration of the cone sheets is highly variable across the complex, with relatively unaltered sheets often juxtaposed with severely altered ones (e.g. GC249 and GC250). The central syenites are characterized by red Fe-oxide staining and white–brown alteration colours. In total, 33 samples were collected from the intrusive complex, covering all recognizable petrological types and alteration styles. The grid references for the cone sheet and syenite sample sites are given in Supplementary Data Table 1A (available for downloading at <http://www.petrology.oxfordjournals.org/>) and corresponding sample localities are shown in Fig. 2. Three additional samples of apparently unaltered (in outcrop) extra-caldera phonolite dykes were taken from road cuttings near El Risco for comparison (Fig. 1).

ANALYTICAL TECHNIQUES

X-ray diffraction (XRD) analyses were carried out on selected whole-rock samples at the Geochemistry Laboratory in the Geology Department of Trinity College Dublin, Ireland. The minerals present in each powdered sample were determined with a Phillips PW1050/25 diffractometer, using Cu K α radiation. All measurements were taken from 2 to 40° (2 θ) at a step size of 0.02° s⁻¹. X-ray diffractograms were interpreted using ‘Traces 5.20’ software, and identification of minerals was achieved by

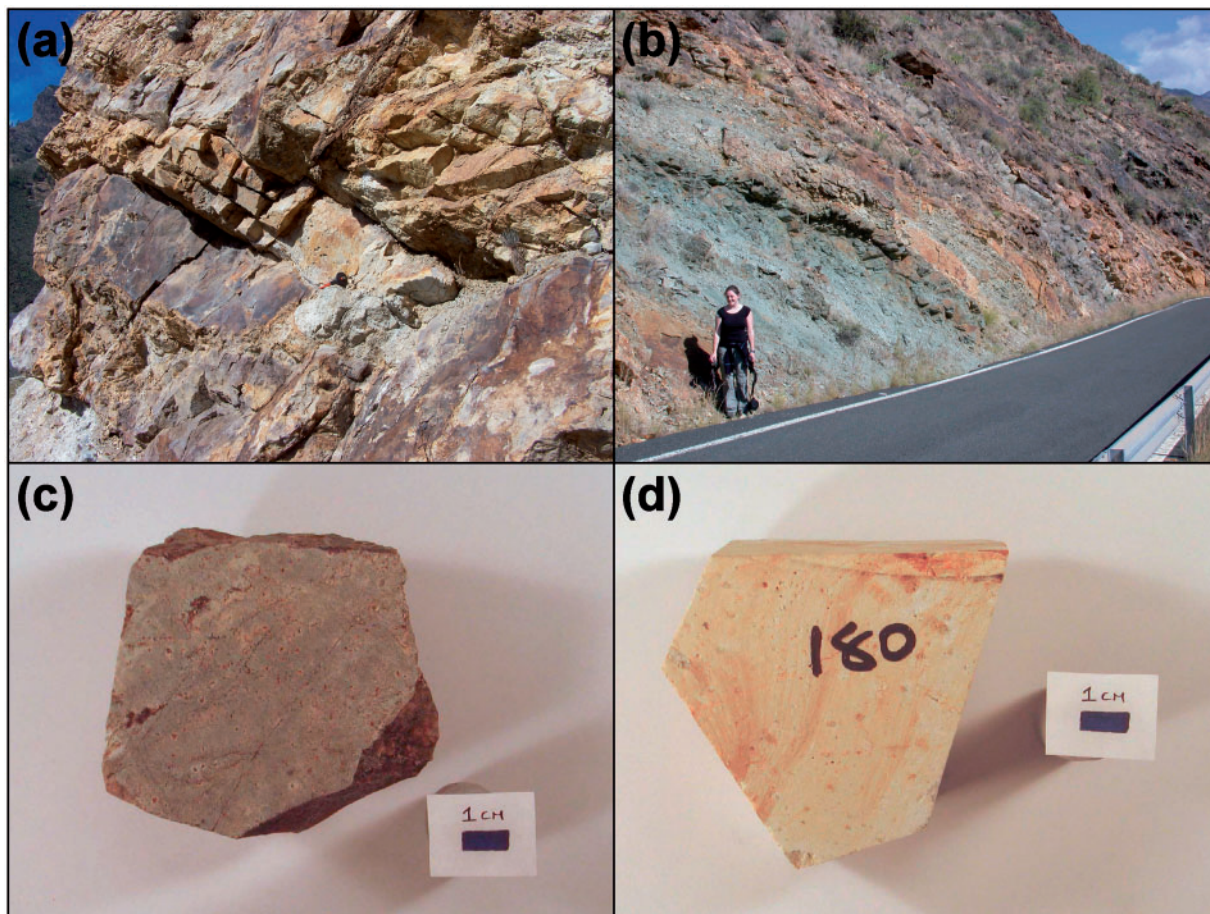


Fig. 4. (a) Hydrothermally altered cone sheets from close to the centre of the cone sheet swarm [431753, 3096640]. It should be noted that alteration appears to be more intense in thinner dykes, and along the contacts between juxtaposed intrusions (paler colours), whereas the central zones portions of thicker dykes are more massive and appear to have escaped major alteration (darker colour). Chisel at centre of image ~ 20 cm. (b) Intensely altered (clay- and zeolite-rich), friable cone sheets from the centre of the cone sheet swarm, displaying extensive alteration. (c) Sample GCl79 displaying Fe–Ti oxide and Mn-oxide veining. (d) Sample GCl80 displaying a bleached appearance and fluidal texture.

comparison of peak angles with the Carleton University Department of Geology 2 θ (Cu) table (Chao, 1969), and the International Centre for Diffraction Data (ICDD) 1998 Powder Diffraction Database (sets 1–48 and 70–85).

Whole-rock major and trace element concentrations were determined by X-ray fluorescence (XRF), using an automated Philips PW1480 spectrometer at IFM-GEOMAR Research Centre, Kiel, Germany. Powdered samples were dried at 110°C prior to analysis, and lithium tetraborate glass fusion beads were prepared according to the methods of Norrish & Hutton (1969), with modifications after Harvey *et al.* (1973) and Schroeder *et al.* (1980). All analyses were carried out with an Rh tube, and calibration was performed using international geological reference samples (see Abratis *et al.*, 2002). Volatile concentrations (H₂O and CO₂) were determined by IR photometry (Rosemount CSA 5003) after heating the rock powder to 960°C.

Whole-rock samples were analysed for their D/H and ¹⁸O/¹⁶O ratios using a Finnigan Delta XP mass spectrometer in the University of Cape Town (UCT), South Africa. All O- and H-isotope data are reported in the familiar ‘ δ ’ notation where $\delta = 1000 \times [(R_{\text{sample}} - R_{\text{standard}}) / R_{\text{standard}}]$ and $R = ^{18}\text{O}/^{16}\text{O}$ or D/H. Powdered samples were prepared for D/H determination off-line, using the method of Vennemann & O’Neil (1993). All samples were degassed on a conventional borosilicate glass vacuum line at 200°C prior to pyrolysis. Water was liberated from 50–100 mg of whole-rock powder, and 100–150 mg of low-blank ‘Indiana’ Zn was used to reduce the liberated water to H₂. For those samples displaying the least amount of secondary alteration in thin section (and therefore expected to be relatively H₂O-poor), 200 mg of sample powder and 200 mg of Zn were used to ensure enough water was liberated and reduced to H₂ for analysis, and to minimize the possibility of contamination of

sample water by blank water in the silicate line. Water was produced from ~50 mg of an internal biotite standard (CGBi, $\delta D = -59\%$, $H_2O^+ = 3.70$ wt %) and analysed in duplicate with each batch of samples. For D/H determination, an internal water standard (CTMP, $\delta D = -9\%$) was used to calibrate the raw data to the V-SMOW scale, and the data were normalized so that V-SLAP gave a value of -428% on the V-SMOW scale, as recommended by Coplen (1995). Water concentrations (H_2O^+) of whole-rocks were determined from the voltage measured on the mass 2 collector of the mass spectrometer, using identical sample inlet volume (Vennemann & O'Neil, 1993). The analytical errors for δD and H_2O^+ are typically of the order of $\pm 2\%$ (1σ) and 0.10 wt % (1σ), respectively, but it should be noted that the error on δD may be somewhat higher in those samples containing low concentrations of H_2O^+ (see Harris *et al.*, 2005) as a result of a greater possibility of blank water contamination during extraction.

For O-isotopes, powdered samples (~10 mg) were dried in an oven at $50^\circ C$, and degassed under vacuum on a conventional silicate line at $200^\circ C$ for 2 h. Silicates were reacted with ClF_3 in the silicate line for 3 h at $550^\circ C$ (Borthwick & Harmon, 1982), and the liberated O_2 was converted to CO_2 using a hot platinumized carbon rod. Further details on the methods employed for O-extraction from silicate minerals at UCT has been given by Vennemann & Smith (1990) and Harris & Erlank (1992). Samples were run on the vacuum line in batches of eight, along with duplicate samples of the internal quartz standard, NBS-28. For $^{18}O/^{16}O$ determination, a $\delta^{18}O$ value for NBS-28 of 9.64% was used to normalize the raw data to the V-SMOW scale (Coplen *et al.*, 1983). The normalized and un-normalized $\delta^{18}O$ values differ by $<0.4\%$. The analytical error for $\delta^{18}O$ is estimated to be about $\pm 0.1\%$ (1σ) for all samples, based on long-term duplication of NBS-28.

RESULTS

Petrography

Petrographic descriptions of cone sheets ($n = 27$), syenite ($n = 3$) and the extra-caldera phonolite dyke ($n = 3$) samples are included in Supplementary Data Table 1A (<http://www.petrology.oxfordjournals.org/>). A summary of the main petrographic features of each sample suite is given below and photomicrographs of selected alteration textures are shown in Fig. 5.

Original magmatic textures of cone sheet samples range from microcrystalline and aphanitic (e.g. GC250) to strongly porphyritic (e.g. GC244). Phenocryst assemblages are dominated by alkali-feldspar (~10 vol. %), with minor Fe–Ti oxide (<5 vol. %), biotite–phlogopite (<2 vol. %), titanite (<1 vol. %), and apatite (<1 vol. %) (see Schirnick, 1996; Schirnick *et al.*, 1999). Alkali-feldspar phenocrysts are subhedral to anhedral, ~0.5–3 mm in

size, and typically display anti-perthitic textures where they have undergone exsolution to albite and orthoclase (Table 1). In the majority of samples, the feldspar phenocrysts display patchy to pervasive turbidity and minor replacement by fine-grained phyllosilicate phases along crystal boundaries, fractures, and twinning planes (e.g. GC243, GC257, GC258; Fig. 5a). Decomposition of Fe–Ti-oxide phenocrysts is prevalent (e.g. GC246, GC177), with many crystals displaying bright red alteration rims (hematite–leucoxene) surrounding relatively unaltered, isotropic cores (Fig. 5b).

Groundmass assemblages in the cone sheet samples are dominated by alkali feldspar, with variable amounts of interstitial Fe–Ti oxide, aegirine, analcime, alkali-amphibole, quartz and glass. Groundmass textures range from variolitic (e.g. GC250), to trachytic (e.g. GC258) to felsitic or cryptocrystalline (e.g. GC249). Groundmass feldspar laths are typically cloudy or turbid (e.g. GC242, GC243, GC261, GC263), and display partial replacement by fine-grained phyllosilicate phases and poorly crystalline Fe–Ti oxides (e.g. GC184, GC181; Fig. 5d). Only one cone sheet sample (GC249) retains a relatively unaltered appearance in thin section (Fig. 5c), and contains primary (unexsolved) anorthoclase (Table 1). Where groundmass analcime is present, it forms isotropic to weakly birefringent crystals in interstices. Alkali-amphibole (arfvedsonite–kaersutite; see Schirnick, 1996) was identified in two relatively unaltered cone sheets (GC249 and GC257), where it forms acicular, blue–green crystals intergrown with aegirine or, more rarely, well-developed, strongly pleochroic prismatic crystals extending into miarolitic cavities (e.g. GC249; Fig. 5c). Where present, both aegirine and alkali-amphibole often display partial alteration to poorly crystalline Fe–Ti oxides (Fig. 5c). Quartz occurs in numerous altered cone sheet samples as a groundmass phase (e.g. GC246), infilling fractures and cavities (e.g. GC250), and as fine-grained, polycrystalline rims around feldspar phenocrysts (e.g. GC177). Precipitation of Mn-oxide dendrites (Fig. 5e), and decomposition of interstitial Fe–Ti-oxides (Fig. 5f), was also observed in numerous cone sheet samples.

The three syenite samples display coarse, holocrystalline textures, and have bulk mineral assemblages comprising mainly alkali feldspar (>60 vol. %), clinopyroxene (<20 vol. %), alkali-amphibole (<5 vol. %), and Fe–Ti-oxide (<5 vol. %). Phlogopite (<10 vol. %) with inclusions of apatite, poorly crystalline aegirine (<2 vol. %) and analcime (<1 vol. %) occurs as a late interstitial phase (Fig. 5g). All syenite samples display intense alteration of primary textures and mineral phases. Alkali feldspar laths are strongly turbid, and in many cases only the outline of the original crystal is recognizable (Fig. 5g). Where the alkali feldspar laths are only partially altered, turbid domains are preferentially developed along crystal

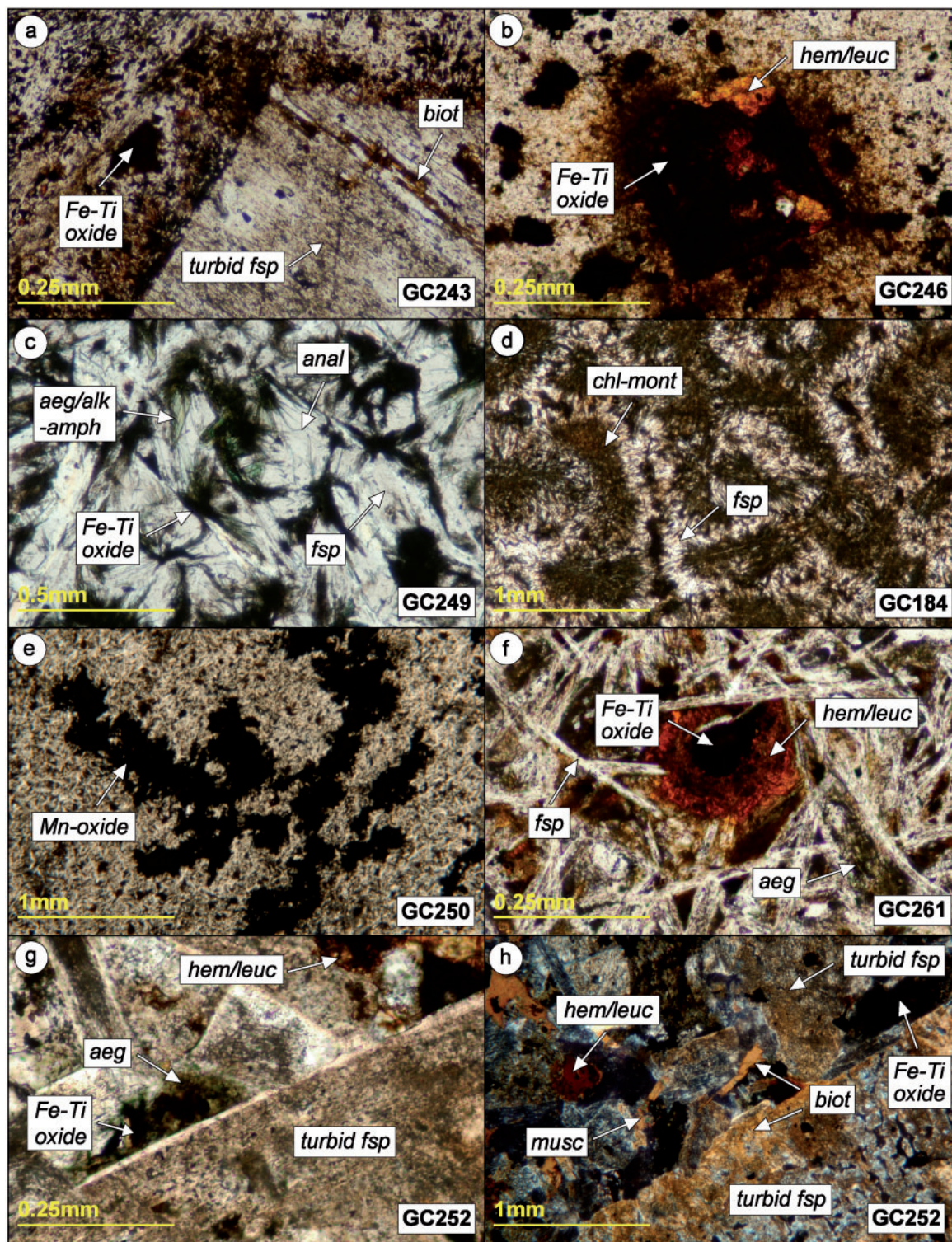


Fig. 5. Photomicrographs of selected cone sheet (a–f) and syenite (g, h) samples. (a) Alkali feldspar phenocryst in GC243 displaying a turbid texture and partial alteration to fine-grained phyllosilicates (chlorite–montmorillonite, biotite) and secondary Fe–Ti oxides along fracture surfaces and crystal boundaries. (b) Fe–Ti oxide phenocryst in GC246 partially decomposed to secondary Fe–Ti (hematite or leucosene). (c) GC249 displaying a relatively unaltered felsitic texture, comprising interlocking alkali feldspar laths, with interstitial aegirine, alkali-amphibole, and analcime. (d) GC184 displaying pervasive replacement of groundmass feldspar by clay minerals (chlorite–montmorillonite). (e) Mn-oxide veins in GC250 displaying a distinctive dendritic texture. (f) Interstitial Fe–Ti oxide in GC261 partially decomposed to secondary hematite–leucosene. (g) GC252 containing strongly turbid alkali feldspar laths, partially decomposed Fe–Ti oxides, and poorly crystalline aegirine overprinted by Fe–Ti oxides in interstices. (h) Alkali feldspar laths in holocrystalline syenite (GC252) displaying well-developed turbidity. Also noteworthy is the alteration of interstitial phases to secondary Fe–Ti oxides, muscovite, and fine-grained phyllosilicates (chlorite–montmorillonite). Magnification $\times 1.2$ for (d), (e), and (h), $\times 5$ for (c), and $\times 10$ for (a), (b), (f) and (g). All photomicrographs taken in plane-polarized light, apart from (h), which is in crossed-polarized light.

Table 1: Primary magmatic, deuteric, and meteoric–hydrothermal mineral assemblages, and corresponding δD , H_2O , $\delta^{18}O$ values, of intra-caldera cone sheets, syenite intrusions, and extra-caldera phonolite dykes

Sample information			Primary magmatic				Late-magmatic–deuteric				Meteoric–hydrothermal			Isotopes		
Sample	Zone	DFC (km)	anorth	K-spar	alb	aeg	anal	alk-amph	phlog	chl-mont	qtz	musc	δD (‰)	H_2O (wt %)	$\delta^{18}O$ (‰)	
<i>Cone sheets</i>																
GC242	ALDZ	6.0		X	X	x					X		−106	0.4	5.5	
GC243	ALDZ	5.4		X	X								−126	0.4	4.9	
GC244	ALDZ	4.8		X	X								−115	0.4	1.7	
GC245	ALDZ	4.8		X	X						x		−123	0.8	2.4	
GC246	ALDZ	4.8		X	X						x		−127	0.5	0.9	
GC247	AHDZ	4.2		X	X						x		−125	0.5	1.8	
GC248	AHDZ	4.2		X	X						X		−129	0.6	2.1	
GC171	AHDZ	4.2		X	X											
GC174	AHDZ	4.2		X	X					x	x		−98	0.8	2.4	
GC249 (fresh)	AHDZ	3.7	X	X		X	X	X					−48, −48	2.4, 2.0	7.1	
GC250	AHDZ	3.7		X	X						x		−107	0.5	4.0	
GC176	AHDZ	3.5		X	X					x	X					
GC177	AHDZ	3.5											−109	0.7		
GC178	AHDZ	3.0											−130, −142	0.5, 0.4	2.1	
GC179	AHDZ	3.0											−149	0.3	0.1	
GC251	AHDZ	2.9		X	X					x			−104	0.5	3.1	
GC255	AHDZ	2.9		X	X					x	x		−97	0.6	4.9	
GC180	AHDZ	2.4		X	X								−108	0.4		
GC181	AHDZ	2.4		X	X					X			−83	0.8	10.0	
GC256	AHDZ	2.3		X	X					x	x		−95	0.7	4.9	
GC257	AHDZ	2.3		X	X	x	x	x		x			−90	0.8	7.2	
GC258	AHDZ	2.3		X	X	x	x			x			−62	0.5	8.6	
GC259	AHDZ	2.3		X	X					x			−117	0.4	3.2	
GC260	AHDZ	1.8		X	X						x		−123	0.5		
GC261	AHDZ	1.8		X	X					x			−100	0.7	8.6	
GC262	AHDZ	1.8		X	X					x			−81	0.7	6.8	
GC263	AHDZ	1.8		X	X	X				x			−89	0.7		
GC184	AHDZ	1.7		X	X					X			−102	0.8	8.4	
GC185	AHDZ	1.7											−108	0.7	8.2	
GC264	AHDZ	1.5		X	X	X				x			−110	0.7		
<i>Syenites</i>																
GC252	AHDZ	2.9		X	X	x			X			x	−91	0.5	2.5	
GC253	AHDZ	2.9		X	X	x							−99	0.5	1.5	
GC254	AHDZ	2.9		X	X	x			x				−121	0.6	0.9	
<i>Extra-caldera phonolite dykes</i>																
GC284	n.a.	10		X	X	X	X	X		x			−59, −53	2.1, 2.1	8.6	
GC285	n.a.	10		X	X	X	X	X					−81, −74	0.9, 2.1	7.5	
GC286	n.a.	10		X	X	X	X	X					−65, −62	1.6, 2.1	7.5	

ALDZ, Annular Low Density Zone; AHD, Annular High Density Zone (see Schmincke, 1998; Schirnick *et al.*, 1999). DFC, 'Distance from Centre', the measured 'straight line' distance of each sample locality from the axis of radial symmetry of the cone sheet swarm (see Schirnick, 1996; Schirnick *et al.*, 1999). Large bold 'X' indicates mineral represented by major peak on XRD scan; small 'x' indicates mineral represented by minor peak on XRD scan. anorth, anorthoclase; K-spar, K-feldspar; alb, albite; aeg, aegirine; anal, analcime; alk-amph, alkali-amphibole; phlog, phlogopite; chl-mont, chlorite–montmorillonite; qtz, quartz; musc, muscovite. n.a., not applicable.

boundaries and fractures, with some samples displaying relatively limpid cores. In GC252, interstitial feldspar is altered to fine-grained muscovite (Fig. 5h), whereas biotite laths and interstitial aegirine are overprinted by conspicuous clusters of opaque crystallites. Decomposition of Fe–Ti oxides to hematite–leucoxene is observed in all three syenite samples (Fig. 5h), whereas dendritic Mn-oxide aggregates are relatively rare, and occur only in the interstices of GC253, where they overprint feldspar.

The three extra-caldera phonolite dykes are generally phenocryst poor (<2 vol. % alkali feldspar) and display either trachytic (GC284 and GC285) or variolitic (GC286) groundmass textures. Groundmass assemblages are dominated by alkali feldspar, with aegirine, analcime, alkali-amphibole, and Fe–Ti oxides as interstitial phases. Small (<0.5 mm wide) miarolitic cavities are common in GC284, and are filled by alkali-amphibole, aegirine, and/or analcime. Despite their relatively unaltered appearance in the field and in hand sample, the extra-caldera phonolite dykes contain turbid groundmass feldspar (e.g. GC285), and show partial replacement of aegirine and amphibole crystallites by fine-grained phyllosilicates and Fe–Ti oxides (e.g. GC284).

X-ray diffraction (XRD)

The mineralogy of each sample suite, as deduced from the whole-rock XRD data, is shown in Table 1. The approximate 'straight-line' distance (in km) of each sampling point from the axis of radial symmetry of the cone sheet swarm (centred around Los Reyos; Schirnack, 1996; Schirnack *et al.*, 1999; Fig. 1), and the O- and H-isotope ratios and H₂O concentrations, are also indicated.

The bulk mineralogy of the extra-caldera phonolite dykes ($n=3$) comprises K-feldspar + albite + aegirine + analcime + alkali-amphibole ± chlorite–montmorillonite. The altered intra-caldera cone sheets ($n=26$) contain K-feldspar + albite ± aegirine ± quartz ± analcime ± alkali-amphibole ± chlorite–montmorillonite, and the altered syenite samples ($n=3$) contain K-feldspar + albite + aegirine ± biotite–phlogopite ± muscovite. It should be noted that albite and K-feldspar are the dominant phases in all samples apart from GC249, which contains anorthoclase. The phyllosilicate phases produced very low-intensity peaks on the majority of the XRD scans, suggesting that clay alteration is not volumetrically significant. Only two cone sheet samples (GC181 and GC184) produced relatively high-intensity peaks at around 3° (2 θ), reflecting the presence of chlorite–montmorillonite in considerable quantities (>5 vol. %). Secondary Fe–Ti oxides, which are visible in nearly all samples in thin section, were not detected by XRD methods, perhaps reflecting their poorly crystalline nature, and/or their relatively low volume.

Major and trace elements

The major element oxide, trace element, and total volatile (H₂O + CO₂) concentrations of the altered cone sheets and syenites, the unaltered cone sheet (GC249), and one relatively unaltered extra-caldera phonolite dyke (GC286) are reported in Table 2. The unaltered cone sheet plots in the phonolite field on a total alkali vs silica (TAS) diagram (Le Maitre *et al.*, 1989; Fig. 6), whereas the altered cone sheets plot in the trachyte field and define an overall trend of decreasing Na₂O + K₂O wt % with increasing SiO₂ wt %. All the plotted data are normalized to 100% on a volatile-free basis. Selected major and trace elements are plotted versus Zr as an index of differentiation in Figs 7 and 8 (Schirnack, 1996). Zr concentrations range from 841 to 1866 ppm in the cone sheets, with the unaltered extra-caldera dyke also plotting within this range (1078 ppm). Zr concentrations in the syenite samples are relatively low and uniform (464 and 476 ppm). In the cone sheets, the majority of the major element oxides (e.g. SiO₂, Al₂O₃, Fe₂O₃, CaO, MgO, MnO) show no systematic variation with Zr concentration; Na₂O and K₂O show weak positive and negative correlations, respectively (Fig. 7f and g). Incompatible trace elements (Nb, Y, Rb, Ce,) all show positive correlations with Zr, with the lowest concentrations consistently observed in the syenites (Fig. 8a–d; similar correlations are also observed for Th, La, and Zn). In contrast, the compatible trace elements (Ti, P, Sr, Ba) are highly concentrated in those samples with the lowest Zr contents (i.e. the syenites), but relatively low and constant in concentration in the cone sheets (Fig. 8e–h). H₂O concentrations range from 0.79 to 1.70 wt % in the altered cone sheets, whereas the syenite samples have H₂O concentrations of 0.72 and 0.86 wt % (Table 2). The unaltered cone sheet and the extra-caldera dyke have relatively high H₂O concentrations of 1.65 and 2.68 wt %, respectively.

Whole-rock O and H isotopes

The O and H isotope compositions and water concentrations of all samples are reported in Table 1. The extra-caldera phonolite dykes have $\delta^{18}\text{O}$ values of 8.6, 7.5, and 7.5‰, which lie at the higher end of the $\delta^{18}\text{O}$ range for 'normal' (i.e. unaltered) trachytes and syenites ($\delta^{18}\text{O}=6\text{--}8\text{‰}$; e.g. Taylor, 1968; Fig. 9). In contrast, the $\delta^{18}\text{O}$ values for the altered intra-caldera cone sheets range from 0.1 to 10.0‰ (average $\delta^{18}\text{O}=4.7\text{‰}$; $n=22$), and can be divided into two groups (Fig. 9; Table 1): (1) samples characterized by low $\delta^{18}\text{O}$ values (0.1–5.5‰) relative to unaltered trachytes and syenites; (2) samples with 'normal' to relatively high $\delta^{18}\text{O}$ values (6.8–10.0‰). The low $\delta^{18}\text{O}$ values correspond to those samples displaying strongly turbid feldspars, but little or no clay replacement (GC242–GC248, GC174, GC178, GC179,

Table 2: Whole-rock major oxide and trace element concentrations (from XRF) for the cone sheets, syenites and an extra-caldera phonolite dyke

Sample name:	GC178	GC181	GC184	GC185	GC242	GC246	GC249	GC252	GC253	GC257	GC258	GC259	GC261	GC286
Sample type:	CS	CS	CS	CS	CS	CS	CS(fr)	SY	SY	CS	CS	CS	CS	PHD
<i>wt %</i>														
SiO ₂	63.31	66.77	62.78	64	62.65	61.19	57.47	58.21	63.26	61.75	60.62	62.85	64.06	61.43
TiO ₂	0.78	0.78	0.92	0.83	1.05	0.76	0.93	1.15	0.7	0.54	0.87	0.72	0.8	0.78
Al ₂ O ₃	17.04	16.64	17.78	17.04	15.81	17.07	16.38	17.53	18.08	16.92	15.43	17.86	16.69	16.37
Fe ₂ O ₃	5.27	2.04	3.41	3.96	5.87	5.83	5.19	4.47	2.69	3.88	6.34	3.32	4.46	4.52
MnO	0.45	0.01	0.16	0.19	0.79	0.37	0.5	0.22	0.18	0.53	0.58	0.1	0.08	0.42
MgO	0.09	0.26	0.34	0.25	0.32	0.13	0.54	1.19	0.14	0.31	0.46	0.11	0.17	0.44
CaO	0.18	0.12	0.23	0.31	0.12	0.29	0.56	2.09	0.48	0.43	0.38	0.39	0.1	0.37
Na ₂ O	5.93	4.8	5.89	6.66	5.96	5.96	9.34	6.98	7.62	7.81	7.14	5.82	6.68	8.28
K ₂ O	6.3	5.98	5.86	5.46	5.38	6.53	5	4.52	4.57	5.27	5.14	7.46	5.66	5.27
P ₂ O ₅	0.05	0.07	0.06	0.04	0.1	0.03	0.08	0.33	0.16	0.03	0.03	0.05	0.03	0.02
Sum	99.68	97.78	97.68	99.13	98.38	98.59	96.36	97.1	98.13	97.86	97.32	98.9	98.97	98.17
CO ₂	0.14	0.11	0.11	0.08	0.09	0.10	0.06	1.40	0.11	0.24	0.77	0.11	0.11	0.07
H ₂ O	0.79	1.57	1.70	1.60	0.65	0.91	2.68	0.72	0.86	1.29	1.47	0.84	0.84	1.65
LOI	0.93	1.68	1.81	1.68	0.74	1.01	2.74	2.12	0.97	1.53	2.24	0.95	0.95	1.72
<i>ppm</i>														
Co	<4	4	n.d.	<4	11	3	1	13	n.d.	8	n.d.	n.d.	n.d.	2
Cr	<18	n.d.	n.d.	<18	n.d.	n.d.	n.d.	n.d.	n.d.	n.d.	n.d.	n.d.	n.d.	n.d.
Ni	<2	n.d.	n.d.	<2	n.d.	n.d.	n.d.	n.d.	n.d.	n.d.	n.d.	n.d.	n.d.	n.d.
V	49	20	23	20	82	100	66	40	27	25	28	33	13	21
Zn	221	157	185	158	279	470	323	117	136	264	269	140	133	181
Ce	401	533	419	502	362	497	545	172	159	495	422	336	341	416
La	201	250	210	250	164	262	262	73	56	218	208	139	144	174
Nb	336	380	280	418	324	458	387	129	131	440	350	274	290	303
Ga	32	36	34	33	44	58	46	28	32	42	41	36	33	34
Pb	18	29	25	21	32	31	29	8	17	31	25	26	32	19
Pr	61	45	39	78	30	44	43	18	12	39	35	27	29	31
Rb	105	197	141	189	143	185	159	76	80	224	173	146	145	139
Ba	52	24	4	11	39	28	31	2173	1092	21	4	34	n.d.	0
Sr	9	13	8	<4	46	10	n.d.	771	176	3	n.d.	4	n.d.	7
Th	25	48	39	27	51	70	52	33	33	64	56	41	42	56
Y	99	66	57	95	73	97	78	27	24	64	77	52	56	53
Zr	1330	1306	831	1677	1390	1857	1479	476	464	1866	1369	841	963	1078

CS, cone sheet; SY, syenite; PHD, phonolite dyke (extra-caldera); fr, fresh. n.d., not detected.

GC250, GC251, GC255, GC256, GC259). The ‘normal’ to high $\delta^{18}\text{O}$ values correspond to samples containing turbid feldspars, partially altered deuteric mineral phases (GC257, GC258), and/or detectable (by XRD) quantities of chlorite–montmorillonite (GC261, GC262, GC181, GC184, GC185). It should be noted that, overall, the highest $\delta^{18}\text{O}$ values occur in those samples from the central part of the intrusive complex (Fig. 10). The petrographically unaltered cone sheet (GC249) has a typical

‘igneous’ $\delta^{18}\text{O}$ value of 7.1‰. The three central syenite samples have consistently low $\delta^{18}\text{O}$ values of 2.5, 1.5, and 0.9‰.

The extra-caldera phonolite dykes have δD values of –59, –81, and –65‰, which are within the typical δD range for hydrous minerals from unaltered igneous rocks ($\delta\text{D} = -55$ to -85 ‰; Taylor, 1968, 1974; Figs 9 and 11). The δD values of the altered intra-caldera cone sheets range from –62 to -149 ‰ (average $\delta\text{D} = -108$ ‰; $n = 28$), and

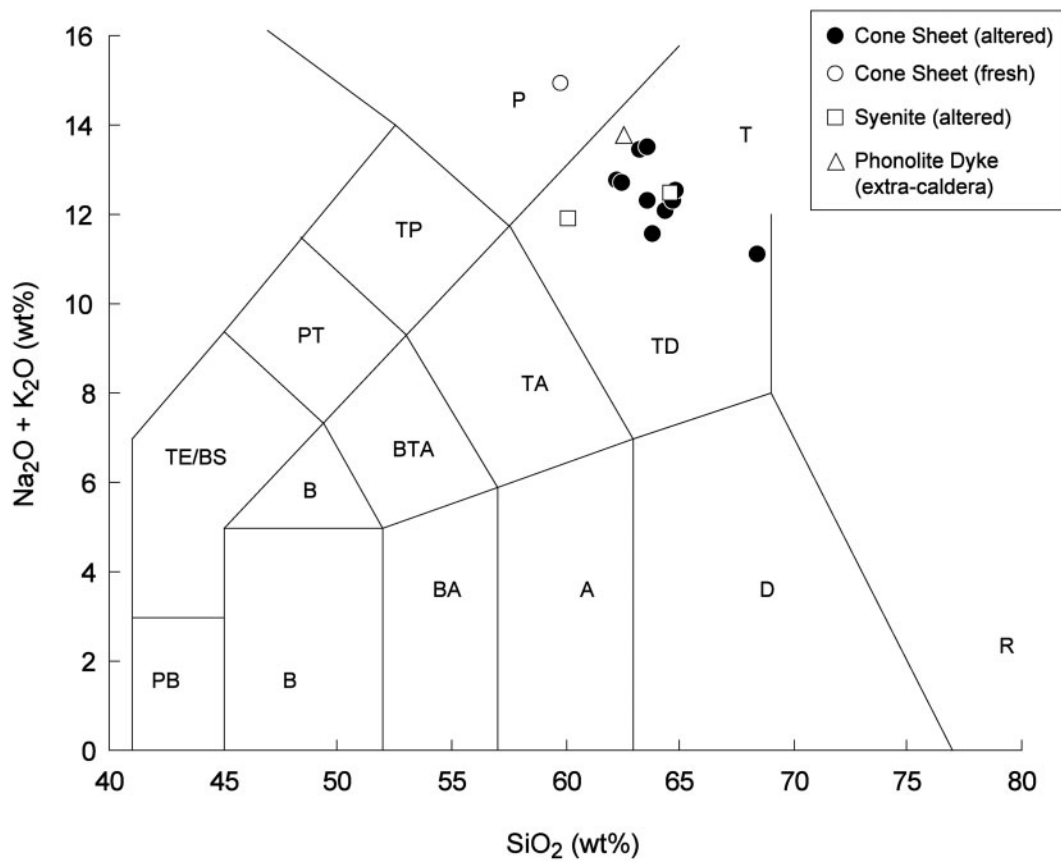


Fig. 6. Total alkali vs silica (TAS) diagram (Le Maitre *et al.*, 1989) showing the classification of the altered cone sheets and syenites, the unaltered cone sheet (GC249), and a relatively unaltered extra-caldera dyke (GC286). PB, picro-basalt; B, basalt; BA, basaltic-andesite; A, andesite; D, dacite; R, rhyolite; BTA, basaltic trachyandesite; TA, trachyandesite; TD, trachydacite; T, trachyte; TE, tephrite; BS, basanite; PT, phono-tephrite; TP, tephri-phonolite; P, phonolite. (See text for details.)

extend down to much more negative values than those of the extra-caldera dykes and the unaltered intra-caldera cone sheet (GC249, $\delta D = -48\text{‰}$). The H_2O^+ concentrations of the extra-caldera dykes (2.1, 0.9, and 1.6 wt %), and the unaltered cone sheet (2.2 wt %), are relatively high compared with the altered cone sheets (0.2–0.8 wt % H_2O^+ ; $n = 28$; Fig. 11). The three central syenite samples have δD values of -91 , -99 , and -121‰ , and corresponding H_2O^+ concentrations of 0.5, 0.5, and 0.6 wt %. The H_2O data obtained from voltage readings on the mass spectrometer during δD analyses (Table 1) are consistent with the H_2O concentrations determined by IR photometry (Table 2). The highest H_2O concentrations occur in the relatively unaltered samples containing hydrous deuterium minerals (e.g. GC249, GC257, GC258, GC286), and in altered samples containing significant quantities of chlorite–montmorillonite (e.g. GC181, GC184; Table 1), whereas lower H_2O concentrations occur in the altered cone sheets (e.g. GC178, GC242) and syenites (GC252, GC253) containing strongly turbid feldspars.

DISCUSSION

Petrography, mineralogy, and paragenetic sequence

The minerals present in each sample have been classified as either ‘primary magmatic’ (i.e. those minerals that grew in the presence of a silicate melt, with or without a coexisting fluid phase), ‘deuteric’ (i.e. those minerals that crystallized directly from fluids exsolved from the melt during the final stages of solidification, or that precipitated as a result of interaction between such fluids and pre-existing primary magmatic phases), or ‘secondary meteoric–hydrothermal’ (i.e. those minerals that formed as a result of solid-state reactions between primary magmatic or deuteric mineral phases and heated meteoric fluids) (see Table 1).

Primary magmatic mineral phases

The petrographically unaltered intra-caldera cone sheet sample (GC249) provides a good first-order approximation of the primary magmatic mineralogy of the altered cone

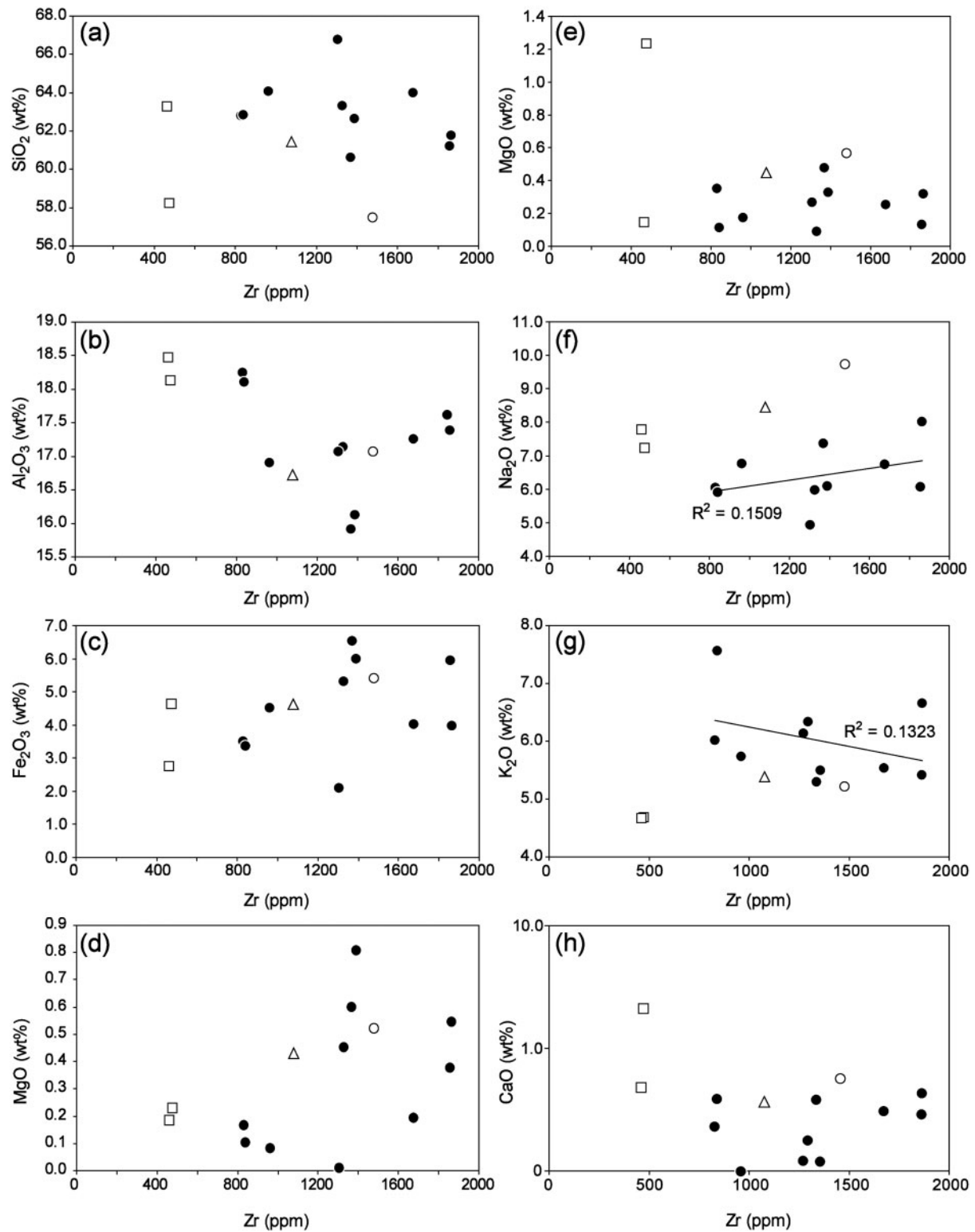


Fig. 7. Plots of selected major element oxides (Si, Al, Fe, Na, K, Ca) vs Zr for the altered cone sheets and syenites, the unaltered cone sheet (GC249), and one relatively unaltered extra-caldera phonolite dyke (GC286). Key as in Fig. 6. Use of log-scale in (h) should be noted. (See text for details.)

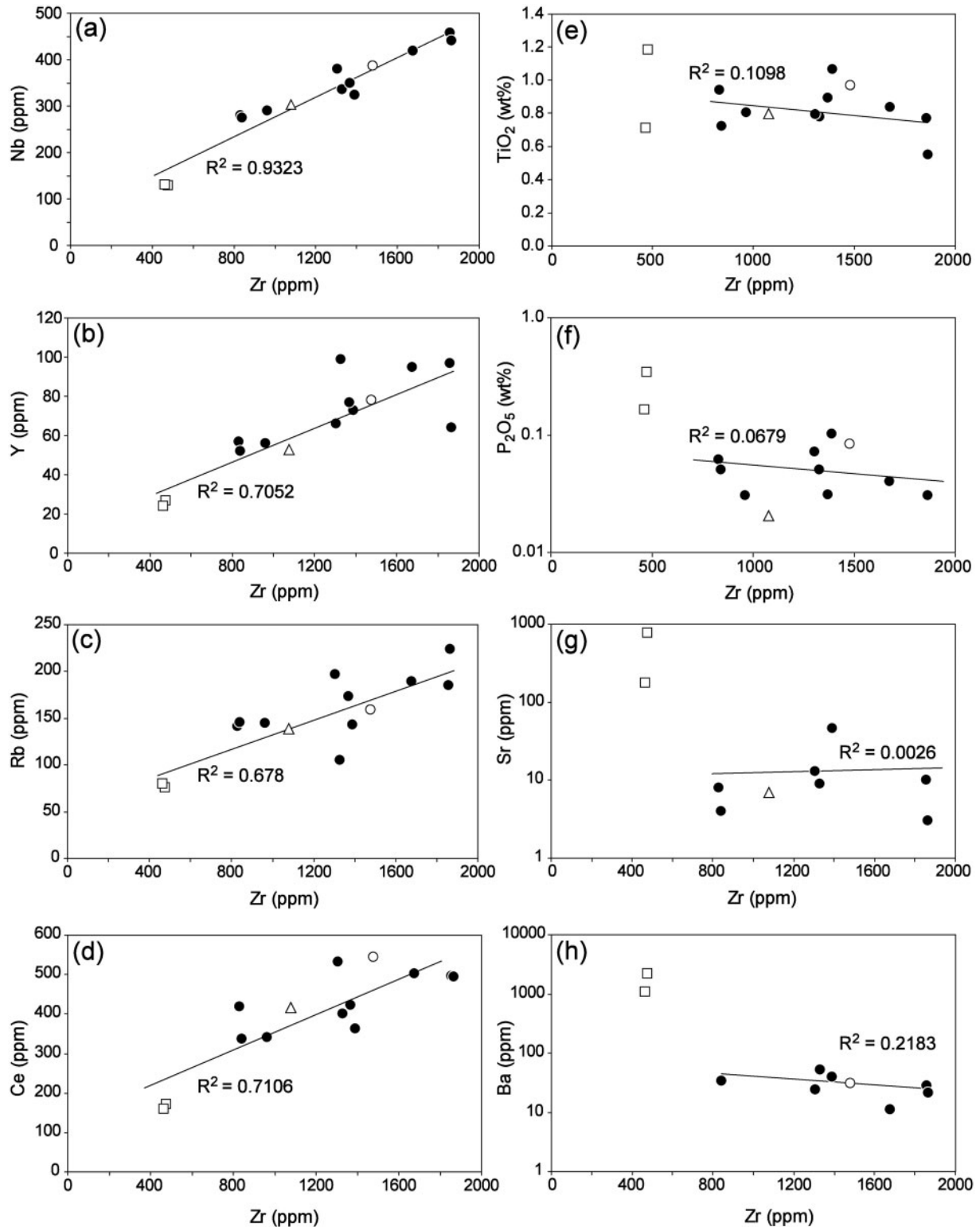


Fig. 8. Plots of selected incompatible (Nb, Y, Rb, and Ce) and compatible (Ti, P, Sr, and Ba) trace elements vs Zr for the altered cone sheets and syenites, the unaltered cone sheet (GC249) and one relatively unaltered extra-caldera phonolite dyke (GC286). Key as in Fig. 6. Best-fit trend lines and R^2 values in (a)–(d) include all data points. Best-fit trend lines and R^2 values in (e)–(h) exclude syenites. Use of log-scale in (f)–(h) should be noted. (See text for details.)

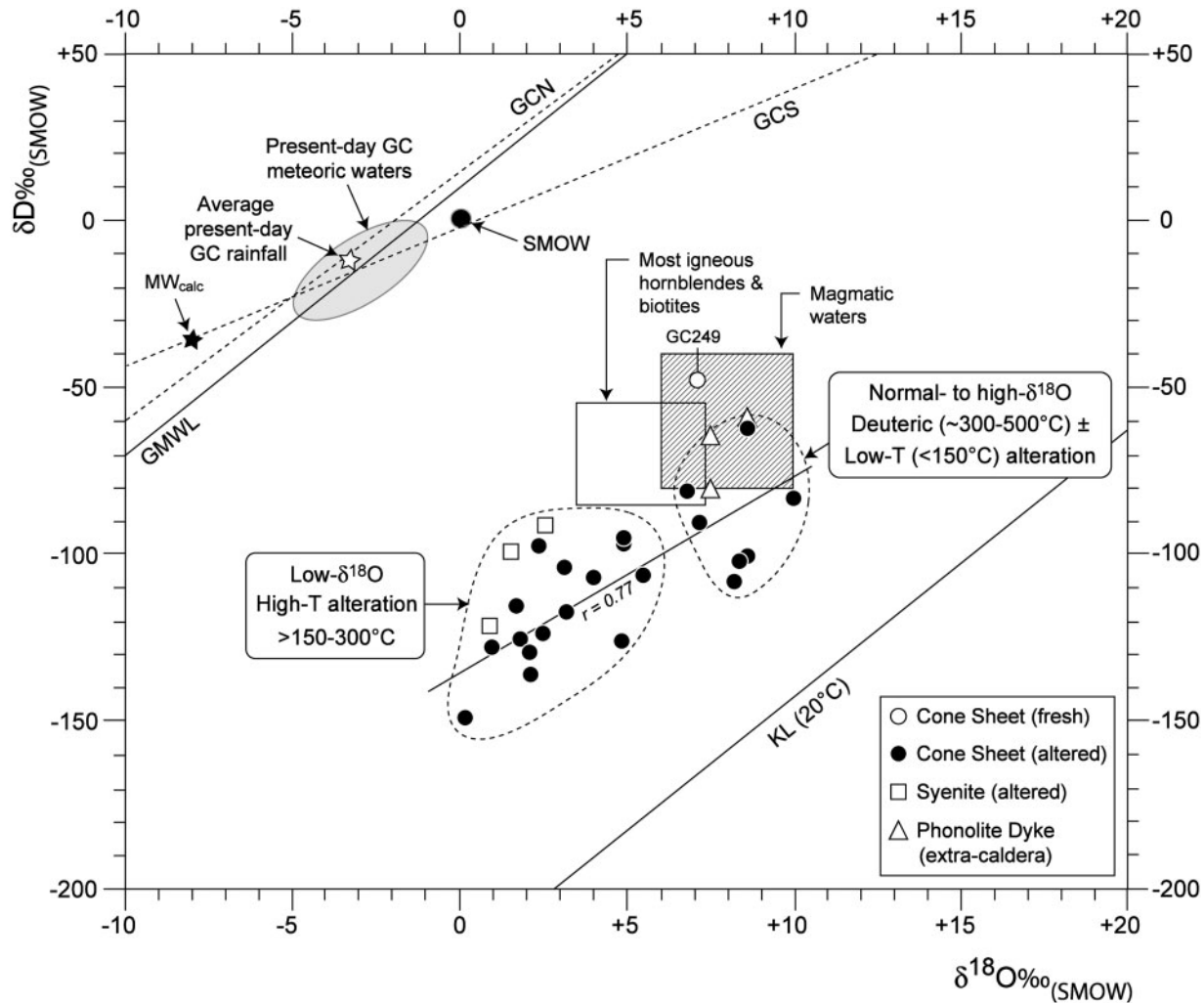


Fig. 9. Whole-rock δD vs $\delta^{18}O$ plot for the altered cone sheets and syenites, the unaltered cone sheet (GC249), and the apparently unaltered extra-caldera phonolite dykes. Also shown for reference are: the Global Meteoric Water Line (GMWL) (Craig, 1961), the local meteoric water lines for north (GCN) and south (GCS) Gran Canaria (Gonfiantini, 1973), the 'kaolinite line' (KL) (Savin & Epstein, 1970), the fields for present-day meteoric water on Gran Canaria (Gonfiantini, 1973; Gasparini *et al.*, 1990; Muñoz Sanz, 2005), magmatic waters (Sheppard, 1986a), Standard Mean Ocean Water (SMOW) (Sheppard, 1986a), and most igneous hornblendes and biotites (e.g. Taylor, 1968, 1974; Taylor & Sheppard, 1986), the average composition of present-day precipitation on Gran Canaria ($\delta D = -13\text{‰}$, $\delta^{18}O = -3\text{‰}$), and the estimated composition of meteoric water at the time of alteration (MW_{calc} : $\delta D = -36\text{‰}$, $\delta^{18}O = -8\text{‰}$). The majority of samples have low $\delta^{18}O$ values relative to the unaltered cone sheet, reflecting the effects of high-temperature, meteoric–hydrothermal alteration. Seven samples have 'normal' to relatively high $\delta^{18}O$ values, reflecting variable degrees of deuteric and/or low-temperature, meteoric–hydrothermal alteration. The range of δD values in the altered cone sheets can be attributed to variable degrees of magmatic degassing, thermal metamorphism, and/or retrograde hydrothermal alteration. The unaltered cone sheet and extra-caldera dykes preserve relatively high (undegassed) δD values. The positive $\delta^{18}O$ – δD correlation ($r = 0.77$) in the altered cone sheets, which approximately parallels the GMWL, is most probably fortuitous, and simply reflects the two data groups (high $\delta^{18}O$ and low $\delta^{18}O$). (See text for details).

sheets. In this sample, high-temperature alkali feldspar (anorthoclase) is the dominant primary mineral phase, together with variable amounts of Fe–Ti oxide and minor accessory phases (titanite, apatite). It should be noted that in all other samples, anorthoclase has exsolved to K-feldspar and albite (Table 1). Although fluid–feldspar interactions may play a role in the exsolution process (e.g. Worden *et al.*, 1990; Witt-Eickschen *et al.*, 1996), there are insufficient petrographic data available for the present

sample set to specify whether exsolution took place under dry or wet conditions. For the purposes of this study, K-feldspar and albite are also considered primary magmatic phases.

Deuteric mineral phases

Aegirine occurs as an interstitial phase in numerous cone sheets (including GC249; Fig. 5c), and in all syenites and the extra-caldera phonolite dykes (Table 1). Similar

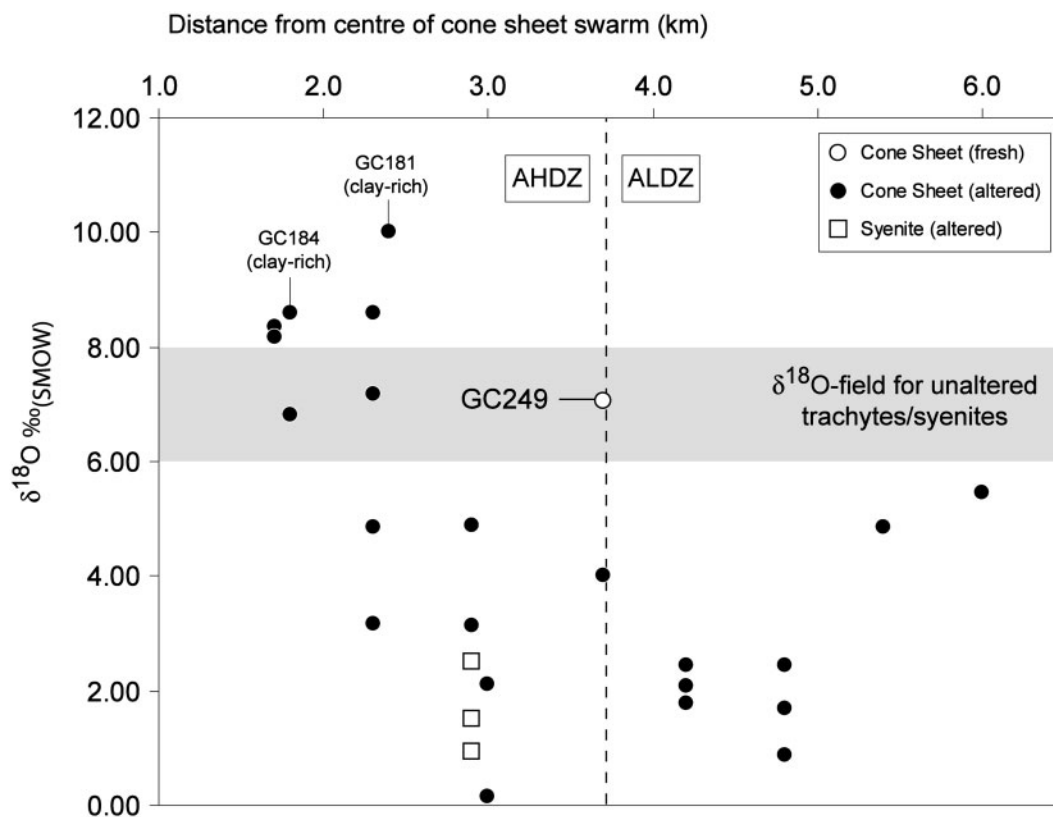


Fig. 10. Plot of whole-rock $\delta^{18}\text{O}$ vs approximate 'straight-line' distance of each sample locality from the central axis of radial symmetry of the cone sheet swarm (see Schirnick *et al.*, 1999). Also shown for reference is the $\delta^{18}\text{O}$ field for unaltered trachytes and syenites ($\delta^{18}\text{O} = 6\text{--}8\text{‰}$; e.g. Taylor, 1968). A noteworthy feature is the lack of any systematic variation in $\delta^{18}\text{O}$ with distance across the intrusive complex, reflecting overprinting of isotopic compositions as a result of multiple cone sheet intrusions over ~ 5 Myr. Overall, however, the highest $\delta^{18}\text{O}$ values occur in relatively clay-rich dykes closer to the centre of the cone sheet swarm, suggesting enhanced retrograde alteration at the centre of the intrusive complex. (See text for details.)

occurrences of interstitial aegirine have been described by Marks *et al.* (2003) from the peralkaline syenites and alkali granites of the Puklen complex (Gardar Province, south Greenland), where its formation is associated with deuteric alteration of Ca-bearing phases by late magmatic, Na-rich aqueous fluids at temperatures $< 300^\circ\text{C}$, and under relatively oxidizing conditions [$f\text{O}_2$ between the FMQ (fayalite–magnetite–quartz) and HM (hematite–magnetite) buffers]. Studies of other intrusive complexes in the Gardar Province (e.g. Klokken, Ilímaussaq) have also shown that late-stage fluids expelled from alkaline to peralkaline intrusions are typically highly enriched in alkali elements (Parsons *et al.*, 1991; Markl, 2001; Markl & Baumgartner, 2002; Schönenberger *et al.*, 2006). In our samples, the dominantly interstitial occurrence of aegirine, and its close association with other sodic (arfvedsonite–kaersutite) and hydrous (analcime) mineral phases, is consistent with crystallization from Na-rich deuteric fluids, released during the final stages of solidification. However, it should be noted that aegirine and alkali-amphibole may also grow directly from silicate

melts (i.e. as primary magmatic phases), as shown by their occurrence as quenched needles in glass-bearing syenite xenoliths from Tenerife (Wolff, 1987; Wolff & Toney, 1993). Based on petrographic evidence, a primary magmatic origin could be invoked for the well-formed aegirine and alkali-amphibole crystals in GC249, where groundmass alkali feldspar has not exsolved to K- and Na-rich domains, and shows no evidence of turbidity or replacement induced by reaction with deuteric or meteoric–hydrothermal fluids (Fig. 5c). In samples containing aegirine and/or alkali-amphibole, but also showing turbid feldspar domains and minor clay alteration (GC284–286, GC257, GC258, GC263), it is plausible that the amphiboles and clinopyroxenes are primary igneous phases that remained stable over a range of conditions encompassing both magmatic and hydrothermal temperatures, and were left partially intact by sub-solidus alteration episodes.

Analcime is a common interstitial phase in both the extra-caldera phonolite dykes and the petrographically unaltered cone sheet (GC249; Fig. 5c). The origin of

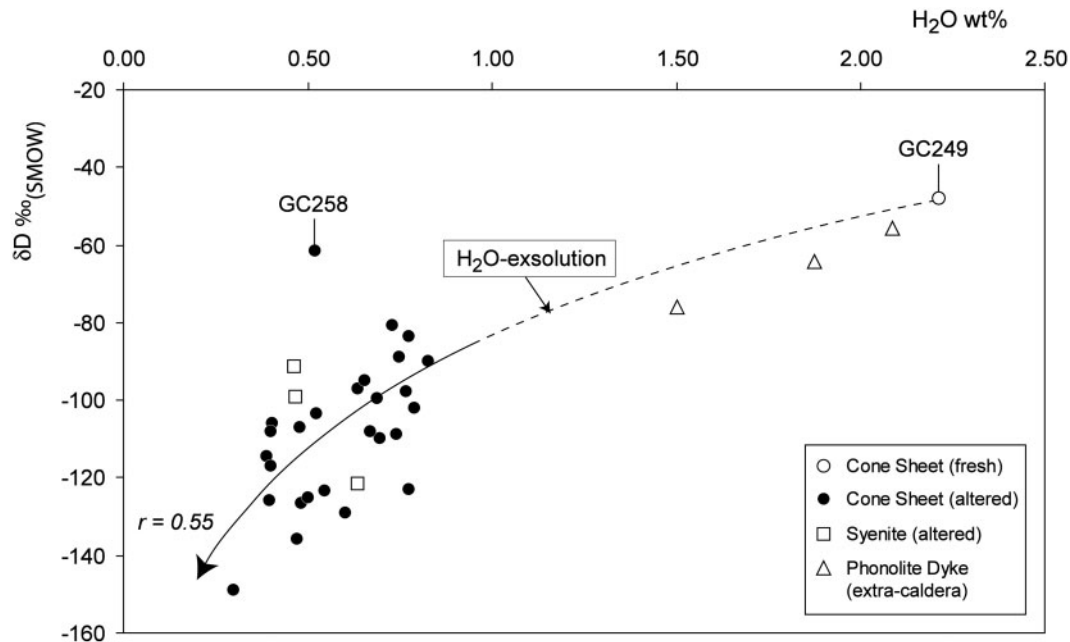


Fig. 11. Whole-rock δD vs H_2O^+ plot for the altered cone sheets and syenites, the unaltered cone sheet (GC249), and the apparently unaltered extra-caldera phonolite dykes. The altered cone sheets have distinctly lower δD and H_2O^+ values than the unaltered cone sheet, and show a weak correlation between δD and H_2O^+ ($r = 0.55$), reflecting the combined effects of Rayleigh-type magmatic H_2O -exsolution (Nabelek *et al.*, 1983; Taylor *et al.*, 1983) and subsequent overprinting of isotopic compositions owing to meteoric–hydrothermal alteration. Sample GC258 has a distinctly higher δD value (-62‰) than the rest of the altered cone sheets, perhaps reflecting retrograde equilibration of clay minerals with present-day meteoric waters ($\delta\text{D} = -20\text{‰}$) during low-temperature weathering. Plotted H_2O^+ data were derived from the voltage measured on the mass spectrometer during H-isotope analysis. (See text for details.)

phenocrystic analcime in alkaline volcanic rocks has long been debated in the literature, with some researchers reporting it as a primary magmatic phase crystallized directly from a hydrous, Na-bearing melt (e.g. Wilkinson 1968; Luhr & Kyser, 1989; Goble *et al.* 1993; Pearce, 1993), and others interpreting it as a replacement product of primary phenocryst phases such as leucite and nepheline, which have interacted with Na-bearing, late magmatic (deuteric) fluids (e.g. Gupta & Fyfe, 1975; Luhr & Giannetti, 1987; Horvath & Gault, 1990). Schirnack (1996) reported rare hexagonal crystallites in some of the younger generation cone sheets in the Tejada Intrusive Complex, which he suggested may have been primary analcime phenocrysts that are now completely replaced. However, the dominantly interstitial occurrence of analcime in our samples suggests that it is a secondary (deuteric) mineral phase, formed by the reaction of late-magmatic, Na-bearing fluids with Si-rich groundmass minerals (e.g. nepheline) or glass (see Peters *et al.*, 1966; Kim & Burley, 1971; Wilkinson & Hensel, 1994). This interpretation is in agreement with the experimental work of Roux & Hamilton (1976), which shows that analcime is only a liquidus phase under very restricted P – T conditions (640 – 600°C ; 5 – 13 kbar), which are inappropriate in high-level alkaline dykes and sills.

Hydrothermal mineral phases

Primary Fe–Ti oxide minerals (e.g. ilmenite, magnetite) and titanite occur both as phenocrysts and as interstitial phases in all cone sheets, and to a lesser extent in the central syenites. In most samples, primary Fe–Ti oxides have undergone partial to complete decomposition to secondary Fe–Ti-bearing phases. The poorly crystalline, red alteration rims around many opaque phenocrysts and interstitial crystals (Fig. 5b and f) are most probably composed of a mixture of hematite and fine-grained leucoxene (see Schirnack, 1996), reflecting the release of Fe and/or Ti during low-temperature exsolution of primary magnetite and/or ilmenite. Secondary Fe-oxide phases occur as fine-grained, opaque disseminations or vein fills in some cone sheets, reflecting the release of Fe into solution from, for example, Fe-rich groundmass phases (e.g. phyllosilicates, aegirine), and subsequent oxidation of Fe by H_2O in fractures. Mn-oxide minerals are also present in many of the cone sheets (and to a lesser extent in the syenites), where they form brown–black, dendritic aggregates coating the surface of the rock (e.g. GC250; Fig. 5e). The dendritic structure of the Mn-oxide deposits is a particularly characteristic feature of pyrolusite (MnO_2) and manganite (MnOOH), both of which commonly occur in hydrothermally altered rocks as low-temperature vein deposits,

or as pseudomorphs after other Mn-oxide minerals (e.g. Post, 1999). Fine-grained phyllosilicate phases (dominantly smectitic clays, e.g. chlorite–montmorillonite) occur in the majority of the cone sheets in minor quantities, and are generally more prevalent in dykes from the centre of the cone sheet swarm (GC181, GC184, GC185; Table 1). Smectitic clays typically occur as replacement minerals above zones of shallow-level epithermal mineralization, in the presence of near-neutral to mildly alkaline (pH ~6–8) hydrothermal fluids up to ~230°C (e.g. Brown & Ellis, 1970; Thompson & Thompson, 1996). Thus, the combination of Mn-dendrites, secondary Fe–Ti oxides, and phyllosilicates in the cone sheets and syenites is consistent with low-temperature, retrograde fluid–rock interaction, most probably related to the influx of relatively cool meteoric waters (see below). Similarly, the groundmass quartz, quartz veinlets, and quartz overgrowths identified in a number of cone sheets (Table 1) can be best explained by low-temperature silicification by quartz-saturated hydrothermal fluids following solidification and fracturing of the intrusive complex (see White & Hedenquist, 1990). The presence of muscovite in GC252 suggests that higher fluid temperatures prevailed during retrograde alteration of the syenites (>300°C; see Deer *et al.*, 1966; Thompson & Thompson, 1996), consistent with their relatively deep position at the core of the intrusive complex (Schirnick *et al.*, 1999).

Overall, the occurrence of late magmatic, hydrous mineral phases, and secondary Fe–Ti–Mn oxides, quartz, and phyllosilicates, provides conclusive evidence that the Tejeda Intrusive Complex underwent significant fluid–rock interaction during the final stages of magmatic crystallization and subsequent solidification. The textures identified (e.g. turbidity, veining, alteration haloes) are consistent with alteration under sub-solidus conditions, either by dissolution and re-precipitation of pre-existing primary phases, or by direct precipitation of secondary minerals from deuteric and/or hydrothermal fluids in micro-fractures and cavities. Experimental studies of melting relations in alkaline rocks (e.g. Edgar & Parker, 1974; Kogarko & Romanchev, 1977; Scaillet & Macdonald, 2001) show that silica under- and over-saturated peralkaline liquids have crystallization intervals ranging from ~800°C down to ~500°C, and typically release alkali-enriched magmatic fluids during the final stages of solidification, at temperatures between 300 and 500°C (see Markl & Baumgartner, 2002; Marks *et al.*, 2003). Thus, the paragenetic sequence observed in the cone sheets and syenites most likely reflects at least three (probably overlapping) phases of fluid–rock interaction: (1) deuteric alteration (~300–500°C) by late magmatic fluids expelled from a solidifying crystal mush (precipitation of analcime, alkali-amphibole, and aegirine); (2) hydrothermal alteration (≥150–300°C) by meteoric water during

the final stages of crystallization and/or immediately following solidification and fracturing of the intrusive complex (development of turbid alkali feldspar and precipitation of secondary muscovite in the syenites); (3) retrograde alteration by relatively cool (≤150°C) meteoric water (minor clay alteration, silicification, decomposition of primary Fe–Ti oxides, and Mn-oxide precipitation). The origins of the hydrothermal fluids, and the temperature ranges for alteration quoted above, are discussed in more detail below, in light of O- and H-isotope data.

Major and trace elements

All major element oxide and trace element concentrations for the samples analysed in this study plot within the ranges reported by Schirnick (1996) for unaltered cone sheets and syenites. Thus, major element mobilization as a result of deuteric or hydrothermal alteration is not considered to be significant in our samples, and the observed elemental variations are thought to largely reflect primary igneous processes. The relatively low concentrations of incompatible trace elements (Th, Y, Rb, Ce, Nb, La, Zn, and Zr), and the relatively high concentrations of compatible trace elements (Ti, Sr, Ba, P) in the syenites compared with the cone sheets (Fig. 8a–h), is consistent with the syenites being the cumulate residue resulting from fractional crystallization of the cone sheet magmas (see Schirnick, 1996; Schirnick *et al.*, 1999). Partitioning of Ba and Sr into feldspar, Ti into Fe–Ti oxides (ilmenite), and P into apatite during fractional crystallization can account for the relatively low concentrations of these compatible trace elements in the cone sheets compared with the syenites (see Schirnick, 1996).

O- and H-isotopes

The final isotopic composition of a rock after fluid–rock interaction is controlled by (1) the initial isotopic composition of the fluid, (2) the initial isotopic composition of the rock, (3) the temperature of the fluid, (4) the water to rock ratio, and (5) the duration (i.e. the approach to isotopic equilibrium) of fluid–rock interaction (e.g. Taylor, 1997). Whereas the whole-rock O- and H-isotope data presented in this study do not allow us to quantify precisely the relative influence of each of these factors, they nevertheless provide valuable insights into the nature of the hydrothermal fluid source, and its isotopic and thermal evolution during fluid–rock interaction. In the Tejeda Intrusive Complex, the dominant hydrothermal fluid source and its initial isotopic composition can be estimated from the whole-rock δD and $\delta^{18}O$ values of the altered cone sheets, and the composition of ambient rainfall for Gran Canaria (see below). The starting rock $\delta^{18}O$ value is assumed to be that of the unaltered phonolite.

Initial water composition

Present-day groundwater on Gran Canaria is recharged at an average altitude of ~ 1000 m above sea level (a.s.l.), and has $\delta^{18}\text{O}$ and δD values ranging from around -1 to -5‰ , and from around -1 to -30‰ , respectively (Gonfiantini, 1973; Gasparini *et al.*, 1990; Muñoz Sanz, 2005). Prior to cone sheet emplacement (during Miocene epithermal activity; 13–12.5 Ma), the average recharge altitude of local meteoric water is thought to have been ~ 400 m a.s.l., corresponding to $\delta^{18}\text{O}$ and δD values of approximately -3 and -15‰ , respectively (Donoghue *et al.*, 2008). Le Bas (1971) has shown that cone sheet intrusions are capable of producing considerable uplift of the overlying country rocks, of the order of several hundred metres. Schirnick *et al.* (1999) suggested that emplacement of the Tejeda Intrusive Complex resulted in a cumulative uplift of more than 2 km over a period of ~ 5 Myr. Thus, it is estimated that the recharge altitude of meteoric water at the time of cone sheet and syenite intrusion was at least 2500 m a.s.l. It is well known that the δD and $\delta^{18}\text{O}$ values of precipitation decrease with increasing altitude (e.g. Dansgaard, 1964). Therefore, a recharge altitude of 2500 m a.s.l. on Gran Canaria would have resulted in a meteoric water source with substantially lower δD and $\delta^{18}\text{O}$ values than present-day precipitation, and lower values than meteoric water feeding the Miocene epithermal system. Using the $\delta^{18}\text{O}$ –altitude correlation and the local meteoric water line for southern Gran Canaria (Gonfiantini, 1973), a $\delta^{18}\text{O}$ value of -8‰ is obtained for a recharge altitude of 2500 m, corresponding to a δD value of -36‰ . It should be noted that the recharge altitude of local precipitation may have been even higher, perhaps >3000 m a.s.l., if a central volcanic edifice similar to, for example, the Plio-Pleistocene Las Cañadas volcano on Tenerife existed above the intrusion (~ 3000 m a.s.l.; see Martí *et al.*, 1994; Ancochea *et al.*, 1999; Carracedo *et al.*, 2007), resulting in even lower $\delta^{18}\text{O}$ and δD values for meteoric water. The presence of a volcanic edifice is not unreasonable, given the large volume of material erupted during the lifetime of the Tejeda intrusive complex (>500 km³ of trachy-phonolitic ash flows, lava flows, and fallout tephra; see Sumita & Schmincke, 1998). It should be noted also that Javoy *et al.* (1986) invoked the presence of a large volcanic edifice (perhaps as much as 4000 m a.s.l.) on the island of Fuerteventura during Oligocene–Miocene times, to explain anomalously low δD values (down to -113‰) in rocks and minerals from the island's basal complex. However, as a first-order approximation, we assume that meteoric water recharging the hydrothermal system of the Tejeda Intrusive Complex had initial $\delta^{18}\text{O}$ and δD values of around -8 and -36‰ , respectively, based on an estimated minimum recharge altitude of ~ 2500 m a.s.l. It should be noted that the $\delta^{18}\text{O}$ value of the meteoric–hydrothermal fluid would have become more positive as fluid–rock

interaction progressed, as a result of isotopic exchange with the surrounding, relatively ^{18}O -rich country rocks.

Initial rock composition

The three apparently unaltered extra-caldera phonolite dykes have δD values of -59 , -61 , and -85‰ , which lie within the reported δD range for most amphiboles and biotites from unaltered igneous rocks (-55 to -85‰ ; Taylor, 1968, 1974; Fig. 9). However, the corresponding $\delta^{18}\text{O}$ values (7.5 , 7.5 , and 8.6‰) are at the higher end of the typical $\delta^{18}\text{O}$ range reported for unaltered phonolitic or syenitic bodies (6 – 8‰ ; e.g. Taylor, 1968; Lutz *et al.*, 1988; Harris, 1995). Assuming a 'normal' upper mantle $\delta^{18}\text{O}$ value of 5.7‰ (e.g. Eiler, 2001), fractional crystallization of primary magmatic phases (mainly alkali feldspar) cannot account for $\delta^{18}\text{O}$ values as high as 8.6‰ in the extra-caldera dykes, because the maximum expected increase in $\delta^{18}\text{O}$ value is $<1\text{‰}$ (e.g. Bindeman *et al.*, 2004). For analcime, chlorite, and smectite, mineral–water O-isotope fractionations ($\Delta^{18}\text{O}_{\text{mineral-water}}$) are positive at temperatures below $\sim 500^\circ\text{C}$ (Wenner & Taylor, 1971; Karlsson & Clayton, 1990; Sheppard & Gilg, 1996), and increase in magnitude substantially with decreasing temperature. Thus, the slightly elevated $\delta^{18}\text{O}$ values in the extra-caldera phonolite dykes compared with unaltered phonolitic rocks probably reflect the combined effects of fractional crystallization, precipitation of ^{18}O -enriched deuteric phases, and sub-solidus hydrothermal alteration of primary and deuteric mineral phases at relatively low temperature. Consequently, it was not possible, it was not possible to estimate reliably the primary igneous isotopic composition and water concentration of the intra-caldera cone sheets from these samples.

Only one intra-caldera cone sheet sample (GC249; Fig. 5c) preserves clear or limpid anorthoclase feldspar, and appears relatively unaffected by retrograde alteration in thin section. The $\delta^{18}\text{O}$ value of this sample (7.1‰) is within the range typical of unaltered phonolitic or syenitic bodies ($\delta^{18}\text{O} = 6$ – 8‰ ; Fig. 9). As such, sample GC249 provides the most reliable approximation of the $\delta^{18}\text{O}$ value of the cone sheets (and probably also the syenites) prior to hydrothermal alteration ($\sim 7\text{‰}$). The δD value of GC249 ($\delta\text{D} \sim -48\text{‰}$) is also close to the typical range reported for unaltered phonolitic or syenitic rocks ($\delta\text{D} = -55$ to -85‰ ; e.g. Taylor, 1968, 1974; Fig. 9). However, this cannot be considered representative of all cone sheets prior to hydrothermal alteration, as some dykes may have solidified with considerably lower δD values from a more degassed (i.e. H_2O -poor, D-depleted) magma source (see below). Given that the oxygen content of a typical magma is significantly higher than the hydrogen content, magmatic degassing would have had a negligible effect on the O-isotope composition of the bulk system and, therefore, the whole-rock $\delta^{18}\text{O}$ values (see Taylor, 1986; Taylor & Sheppard, 1986).

Isotopic compositions and water concentrations of altered cone sheets and syenites

The altered cone sheets have whole-rock $\delta^{18}\text{O}$ values ranging from 0.1 to 10.0‰ (Table 1; Fig. 9). Fifteen out of a total of 22 samples have relatively low $\delta^{18}\text{O}$ values (≤ 0.1 –5.5‰), compared with typical values for unaltered phonolitic or syenitic bodies (6–8‰), and the unaltered cone sheet (GC249; $\delta^{18}\text{O} = 7.1$ ‰). Similarly, the three syenite samples have consistently low $\delta^{18}\text{O}$ values (2.5, 1.5, and 0.9‰), among the lowest in the entire sample set. Low $\delta^{18}\text{O}$ values (down to -7 ‰) in shallow-level intrusive igneous rocks have been attributed to interaction with meteoric water (e.g. Craig, 1961; Sheppard, 1986a; Taylor, 1997). The ^{18}O depletion may be caused by (1) direct infiltration of meteoric water into the magma (e.g. Friedman *et al.*, 1974; Lipman & Friedman, 1975; Hildreth *et al.*, 1984), (2) partial or wholesale assimilation or melting of hydrothermally altered wall-rocks by the magma (e.g. Larson & Taylor, 1986b; Grunder, 1987; Bacon *et al.*, 1989; Brandriss *et al.*, 1995, 1996; Larson & Geist, 1995; Bindeman & Valley, 2000), or (3) sub-solidus hydrothermal alteration of the rock at high temperature (e.g. Criss & Taylor, 1983; Criss *et al.*, 1984). In the Tejedá Intrusive Complex, the presence of deuteric phases in the cone sheets, syenites and extra-caldera phonolite dykes (anaclite, aegirine, and alkali-amphibole) indicates that interaction with exsolved magmatic aqueous fluids was an important process, and would have influenced the whole-rock $\delta^{18}\text{O}$ values to some extent. However, the positive correlation ($r = 0.77$) between $\delta^{18}\text{O}$ and δD in the altered cone sheets (Fig. 9), which broadly parallels the global meteoric water line (Craig, 1961), suggests that meteoric water (rather than magmatic water or seawater) was the dominant fluid source in the hydrothermal system, and/or that any isotopic evidence of late-magmatic fluid–rock interaction has been largely overprinted by subsequent meteoric–hydrothermal event(s). Alternatively, the similarity in slope of the $\delta^{18}\text{O}$ – δD correlation in the altered cone sheets and the meteoric water line may be fortuitous, and simply reflect the presence of two groups of data (low $\delta^{18}\text{O}$ and normal to high $\delta^{18}\text{O}$), representing high- and low-temperature alteration by meteoric water, respectively (see below). The poor $\delta^{18}\text{O}$ – δD correlation within each data group would suggest that the latter interpretation is correct.

In the absence of mineral isotopic analyses, it is difficult to determine the point in the cooling history of the cone sheets and syenites when meteoric water interacted with, and imparted a low- $\delta^{18}\text{O}$ signature on, the rocks. However, several lines of evidence suggest that the low- $\delta^{18}\text{O}$ values reflect the infiltration of low- $\delta^{18}\text{O}$ meteoric water into the intrusive complex following solidification of the cone sheet and syenite magmas (and/or during the very final stages of crystallization), rather than the

presence of initially low- $\delta^{18}\text{O}$ magmas in the source region. First, Crisp & Spera (1987) reported a typical magmatic $\delta^{18}\text{O}$ value of 5.7‰ for an unaltered anorthoclase phenocryst from a Fataga-age ignimbrite sample on Gran Canaria. Given that the Fataga ignimbrites are derived from the same source as the cone sheet and syenite magmas (i.e. the Fataga magma chamber system; see Schirnick *et al.*, 1999), it is unlikely that this source was already depleted in ^{18}O prior to crystallization. If a low- $\delta^{18}\text{O}$ source existed, low $\delta^{18}\text{O}$ values would be expected not only in the intrusive rocks, but also in unaltered feldspar phenocrysts from the Fataga ignimbrites. Second, the unaltered cone sheet sample (GC249) has a ‘normal’ igneous whole-rock $\delta^{18}\text{O}$ value of 7.1‰. Third, petrographic observations show that alkali feldspar crystals in the majority of cone sheets and syenites (both low- $\delta^{18}\text{O}$ and normal- to high- $\delta^{18}\text{O}$ samples) are characterized by the development of patchy to pervasive turbidity. Turbidity is a ubiquitous feature of alkali feldspars in epizonal intrusions and is believed to reflect the presence of numerous tubular micropores on the crystal surface. These micropores are a diagnostic feature of sub-solidus recrystallization of alkali feldspars in the presence of a fluid phase (Worden *et al.*, 1990; Guthrie & Veblen, 1991; Walker *et al.*, 1995; Putnis *et al.*, 2007; Plümper & Putnis, 2009). In addition, several studies have shown that recrystallization of alkali feldspars and the generation of microporosity or turbidity are accompanied by O-isotope exchange and re-equilibration (e.g. Ferry, 1985b; Elsenheimer & Valley, 1993; Cole *et al.*, 2004; Niedermeier *et al.*, 2009). Thus, the presence of turbid alkali feldspars in the altered cone sheets and syenites provides further evidence that meteoric water infiltration and associated O-isotope exchange were post-crystallization processes, and do not reflect direct or indirect contamination by low- $\delta^{18}\text{O}$ meteoric water during magma genesis.

Petrographic observations indicate that alkali feldspar is the most voluminous primary mineral phase in the cone sheets and syenites. It is widely known that hydrothermal solutions readily exchange with alkali feldspars at high temperatures (O’Neil & Taylor, 1967). The alkali feldspar–water O-isotope fractionation ($\Delta_{\text{alkali feldspar-water}}$) decreases with increasing temperature, such that the $\delta^{18}\text{O}$ of alkali feldspar will always be lower than ‘normal’ igneous values (6–8‰) following interaction with a low- $\delta^{18}\text{O}$ fluid at appreciable temperatures (e.g. in excess of $\sim 150^\circ\text{C}$ for a $\delta^{18}\text{O}_{\text{fluid}}$ of -6 ‰). At temperatures lower than 150°C , $\Delta_{\text{alkali feldspar-water}}$ is large and positive (>12 ‰), such that the $\delta^{18}\text{O}$ value of alkali feldspar will increase relative to magmatic values, for $\delta^{18}\text{O}_{\text{fluid}}$ values down to around -8 ‰. Taking $\delta^{18}\text{O}_{\text{alkali feldspar}}$ as a proxy for $\delta^{18}\text{O}_{\text{whole-rock}}$, and a local meteoric water $\delta^{18}\text{O}$ value of -8 ‰ (see above), the relatively low $\delta^{18}\text{O}$ values in the cone sheet and syenite samples (0.1–5.5‰) can be

explained by sub-solidus alteration of alkali feldspar at temperatures between ~ 140 and 230°C . However, it should be noted that these values are minimum temperature estimates, given that the $\delta^{18}\text{O}$ of meteoric water may have been considerably higher as a result of O-isotope exchange with the relatively ^{18}O -rich country rocks over time. Higher alteration temperatures would be more consistent with previous studies of hydrothermal alteration and the development of turbidity in alkali feldspars. For example, Parsons & Brown (1984) suggested a maximum temperature of 400 – 450°C for the development of turbidity in alkali feldspars in the Klokken intrusion (south Greenland), whereas Ferry (1985*b*) suggested maximum temperatures of 350 – 450°C for hydrothermal alteration of alkali feldspars in Tertiary granites from the Isle of Skye. Furthermore, hydrous alteration minerals (e.g. phyllosilicates) occur only in very minor quantities (or are completely absent) in the majority of low- $\delta^{18}\text{O}$ cone sheet and syenite samples, indicating that the temperature of fluid–rock interaction must have been sufficiently high ($>400^\circ\text{C}$) to prevent the stabilization of these phases. Overall, the syenite samples plot closer to the global meteoric water line than the majority of cone sheet samples [which plot closer to the kaolinite weathering line of Savin & Epstein (1970); Fig. 9], indicating that the syenites experienced the highest alteration temperatures in the intrusive complex. It should be noted that O-isotope exchange between mantle-derived igneous rocks and seawater ($\delta^{18}\text{O} \sim 0\text{‰}$) at high temperatures (300 – 600°C) can also produce relatively low whole-rock $\delta^{18}\text{O}$ values (around 6‰ down to around 0‰) in igneous rocks (Muehlenbachs, 1986). However, for our sample set, seawater can be ruled out as a potential hydrothermal fluid source, as O-isotope exchange would have had to take place at temperatures up to around 640°C to produce whole-rock $\delta^{18}\text{O}$ values as low as 0.1‰ . Such high-temperature fluid–rock interaction is inconsistent with the textures observed in the cone sheets and syenites (e.g. turbid feldspars), which clearly attest to alteration under cooler, sub-solidus conditions.

Five altered cone sheets (GC181, GC261, GC262, GC184, and GC185) have relatively high whole-rock $\delta^{18}\text{O}$ values (6.8 – 10.0‰) (Fig. 9; Table 1), which can be attributed to sub-solidus alteration of alkali feldspar by ambient meteoric water ($\delta^{18}\text{O} = -8\text{‰}$) at (minimum) temperatures between ~ 127 and 96°C . This estimated temperature range is in accordance with petrographic observations, which show that these samples contain turbid alkali feldspars, as well as minerals indicative of low-temperature, retrograde alteration, such as clays (mainly chlorite–montmorillonite), and secondary Fe–Ti oxides (Table 1). It should be noted that the highest $\delta^{18}\text{O}$ values occur in cone sheets from close to the central part of the swarm, consistent with enhanced retrograde alteration in this area (Fig. 10).

Two cone sheets (GC257 and GC258) contain deuteric mineral phases (analcime, aegirine, and alkali-amphibole), turbid alkali feldspars, and subordinate phyllosilicate phases (chlorite–montmorillonite), and are characterized by ‘normal’ or only slightly elevated $\delta^{18}\text{O}$ values (7.2 and 8.6‰ , respectively). As in the extra-caldera phonolite dykes, the $\delta^{18}\text{O}$ values of these rocks most probably reflect the combined effects of fractional crystallization, precipitation of ^{18}O -enriched deuteric phases at high temperature (~ 300 – 500°C), and relatively minor low-temperature retrograde alteration.

The altered cone sheets have whole-rock δD values ranging from -62 to -149‰ , and the altered syenite samples have whole-rock δD values of -91 , -99 , and -121‰ (Table 1; Figs 9 and 11). In both sample suites, the δD values extend down to much lower values than those reported for most igneous hornblendes and biotites (-55 to -85‰ ; e.g. Taylor, 1968, 1974), and for the least altered cone sheet sample (GC249; $\delta\text{D} = -48\text{‰}$). The measured blank associated with the H_2O^+ extraction method is extremely small, but highly negative (there is insufficient gas to measure the δD value accurately). It is therefore possible that the very negative δD values in the altered cone sheets and syenites (which contain $<1\text{ wt } \% \text{H}_2\text{O}^+$) represent a proportionally higher component from the blank. However, duplicate analysis of sample GC178 (see Table 1) indicates that the low δD values are reproducible. Low δD values of a similar or greater magnitude have been reported in hydrous minerals (amphiboles) from a number of other alkaline to peralkaline intrusive complexes, including Ilimaussaq, Greenland (-232‰ ; Marks *et al.*, 2004), Red Wine Complex, Labrador (-160‰ ; Sheppard, 1986*b*), and Norra Karr, Sweden (-130 and -150‰ ; Sheppard, 1986*b*). Proposed explanations for such low δD values in magmatic amphibole in these intrusive complexes include exchange with low δD meteoric–hydrothermal fluids (e.g. Nelve *et al.*, 1994; Brandriss *et al.*, 1995; Agemar *et al.*, 1999), open-system magmatic degassing of water from the parental melt (e.g. Nabelek *et al.*, 1983; Taylor *et al.*, 1983), assimilation of organic sediments (e.g. Sheppard, 1986*b*), and interaction and re-equilibration of amphiboles with D-depleted fluids derived from late magmatic oxidation of internally generated CH_4 and/or H_2 (e.g. Marks *et al.*, 2004). The altered cone sheets of the Tejeda Intrusive Complex preserve an overall trend of decreasing δD value with decreasing H_2O^+ concentration (Fig. 11), suggesting that Rayleigh-type magmatic H_2O -exsolution was a major process contributing to the low whole-rock δD values in these samples (and probably also the syenites, although insufficient data are available to observe a trend). During this process, H_2O vapour exsolution from the crystallizing parental magma would have caused the residual melt, and any late-stage, hydrous phases crystallizing from this melt (e.g. analcime,

alkali-amphibole) to become progressively depleted in D and H_2O (see Nabelek *et al.*, 1983; Taylor *et al.*, 1983; Taylor, 1986). However, the correlation between δD and H_2O^+ is relatively weak ($r = 0.55$), suggesting that any systematic relationship between δD and H_2O^+ caused by magmatic degassing has been partially overprinted by retrograde hydrothermal alteration. Given that $\Delta\text{D}_{\text{smectite-water}}$ ranges from around -40 to -20% between 20 and 150°C (Yeh, 1980), low-temperature formation of smectitic clay minerals in equilibrium with local meteoric water ($\delta\text{D} \sim -36\%$) may have resulted in a slight increase in whole-rock δD values and H_2O^+ concentrations in some samples, from initially very low 'degassed' values. This is supported by the fact that the two most clay-rich samples (GC181, GC184) have among the highest δD values (-83 and -102% , respectively) and H_2O^+ concentrations (0.8 and 0.8 wt %, respectively) in the altered cone sheet sample suite (Table 1). However, given the overall water-poor nature of the altered rocks, it is likely that the effect of smectite formation on the whole-rock δD and H_2O^+ values was relatively minor compared with the effect of magmatic degassing. It is also worth noting that the cone sheets were intruded almost continuously (repose intervals of 5 – 10 kyr) over a relatively long period of time (≥ 5 Myr; Schirnick *et al.*, 1999). Such sustained intrusive activity will have resulted in reheating or metamorphism of already solidified cone sheets, promoting the breakdown of any hydrous deuterium or hydrothermal minerals and further water loss.

In contrast to the altered cone sheets and syenites, the unaltered cone sheet (GC249) and the extra-caldera dykes (GC284, GC285, and GC286) preserve relatively high whole-rock δD values (-48 to -81%) and H_2O^+ concentrations (0.9 – 2.2 wt %), suggesting that these samples crystallized from relatively undegassed magmas (Fig. 11). It is possible that these samples were rapidly quenched upon emplacement at relatively high temperature ($\geq 500^\circ\text{C}$), and that any water released from the magma was trapped in hydrous deuterium phases (e.g. analcime, alkali-amphibole) before being significantly depleted in deuterium. This is consistent with the finely crystalline, aphyric nature of these samples, and the presence of high temperature feldspar in GC249. One altered sample (GC258) has a low H_2O^+ concentration (0.5 wt %), similar to the rest of the altered cone sheets (0.2 – 0.8 wt % H_2O^+), but has an anomalously high δD value of -62% (Fig. 11). Although volumetrically minor, petrographic and XRD results indicate that hydrous minerals are present in this sample (e.g. analcime, chlorite–montmorillonite). Thus, the anomalously high δD value of GC258 may reflect retrograde equilibration of these hydrous phases with present-day meteoric water ($\delta\text{D} = -13\%$), without significant addition of H_2O .

Pattern of meteoric water circulation

The exposed cone sheets and syenite stocks of the Tejada Intrusive Complex intrude ≥ 1000 m of ignimbrites and lava flows of the Fataga Group. At greater depth (1 – 3 km), ignimbrites of the Mogán Group, and underlying shield basalt lavas, form the country rocks for unexposed cone sheets and the associated shallow-level (2 – 3 km) Fataga magma system. The relatively porous and permeable extrusive rocks of the caldera fill, and the underlying, fractured basalt lavas, would have been highly susceptible to infiltration of down-going meteoric waters. The high heat flow generated by successive cone sheet intrusions would have promoted radial inflow of heated groundwaters towards the intrusive complex (see Larson & Taylor, 1986c). This type of flow regime has been invoked for numerous shallow-level, relatively simple (i.e. single-stage and/or short-lived), intrusive complexes affected by meteoric–hydrothermal alteration (e.g. the intrusive complexes of Mull and Skye, NW Scotland), and is typically reflected in a characteristic 'bull's eye' pattern of decreasing $\delta^{18}\text{O}$ in the country rocks towards the intrusion, indicative of increasing fluid temperatures and/or effective water–rock ratios towards the heat source (e.g. Taylor & Forester, 1970; Forester & Taylor, 1976; Criss & Taylor, 1986). This 'bull's eye' pattern is often accompanied by an outward decrease in $\delta^{18}\text{O}$ from the centre to the margin of the intrusion, reflecting enhanced infiltration and circulation of low $\delta^{18}\text{O}$ meteoric–hydrothermal fluids along the contact between the intrusion and its surrounding country rocks (e.g. Forester & Taylor, 1977; Farver & Giletti, 1989). The Tejada Intrusive Complex, in contrast, shows no such systematic spatial variation in $\delta^{18}\text{O}$ (Fig. 10). Schirnick *et al.* (1999) have shown that, apart from the dykes in the ALDZ, which are all part of the older generation cone sheet swarm (12.3 – 9.5 Ma), juxtaposed cone sheets of the younger generation have strikingly different ages, particularly within the AHDZ. The scattered distribution of cone sheet ages within the AHDZ (and supporting structural evidence) led Schirnick *et al.* (1999) to propose a model of cone sheet emplacement involving lateral expansion and contraction of a shallow, laccolith-like Fataga magma chamber system. Although the absence of a systematic $\delta^{18}\text{O}$ –distance correlation may partly be a result of random, fracture-oriented fluid access to the cooling intrusive complex, it is more likely that it is a direct reflection of the highly variable spatial distribution of cone sheet ages. Multiple intrusion of dykes with variable diameters over a period of ~ 5 Myr (combined with the isotopic effects induced by uplift and evolving fluid isotopic composition) would have almost certainly precluded the generation of a systematic spatial $\delta^{18}\text{O}$ pattern in the Tejada Intrusive Complex, and would have overprinted any evidence of enhanced alteration or ^{18}O -depletion that may have existed in the oldest intrusions at the margins of

the cone sheet swarm. Such overprinting of isotopic compositions would not be expected for relatively short-lived plutonic complexes such as those of, for example, the British Tertiary Igneous Province, which were emplaced in less than 1 Myr (see Hamilton *et al.*, 1998; Chambers *et al.*, 2005; Troll *et al.*, 2008).

Whereas no systematic trend in $\delta^{18}\text{O}$ was observed across the Tejeda Intrusive Complex, the highest $\delta^{18}\text{O}$ values occur in intrusions from the central part of the cone sheet swarm (Fig. 10), two of which contain significant quantities of chlorite–montmorillonite (GC181, GC184; Table 1). Schirnack *et al.* (1999) reported that syenite stocks were intruded into the central low-dyke density zone at a relatively late stage in the evolution of the intrusive complex (~ 9 Ma). This late syenite intrusion may have been accompanied by resurgent doming or uplift of the surrounding cone sheets and overlying formations (see Le Bas, 1971; Schirnack *et al.*, 1999), thereby promoting enhanced infiltration of cool meteoric water and associated retrograde clay alteration at low temperature in the central part of the intrusive complex.

Timing of alteration

Pervasive epithermal alteration of marginal volcanic tuffs of approximately mid- to late-Mogán age (~ 13.5 – 13 Ma) in the Tejeda caldera has been attributed to the establishment of a large-scale, meteoric–hydrothermal system coinciding with the emplacement of the Fataga magma chamber between 13 and 12.5 Ma (e.g. Schmincke, 1998; Pérez Torrado *et al.*, 2004; Donoghue *et al.*, 2008). The presence of unaltered Fataga ignimbrites with an eruption age of 12.5 Ma (van den Bogaard & Schmincke, 1998), unconformably overlying altered late Mogán tuffs, suggests that epithermal alteration preceded the main period of Fataga volcanism and emplacement of the Tejeda Intrusive Complex (which intrudes dominantly Fataga volcanic rocks). The meteoric–hydrothermal alteration associated with the Tejeda Intrusive Complex may represent a second pulse of hydrothermal activity, generated and sustained entirely by cone sheet and syenite intrusion, and temporally and spatially distinct from that affecting the marginal rocks of the Mogán-age Tejeda caldera. However, given the close temporal association between epithermal alteration and Fataga magma chamber emplacement, it is more likely that the hydrothermal alteration affecting the Tejeda Intrusive Complex represents inward-cooling or ‘shrinking’ of a single large-scale, long-lived hydrothermal system that once extended to the caldera margin during initial Fataga magma chamber emplacement (see Schmincke, 1998). The apparently unaltered Fataga ignimbrites at the margin of the Tejeda caldera may have simply ‘escaped’ hydrothermal fluid-circulation as the hydrothermal system infiltrated the cooling intrusive complex during and after Fataga

volcanism. Schirnack *et al.* (1999) placed an upper limit of 9.5 Ma on hydrothermal activity associated with the intrusive complex, based on the presence of altered feldspars only in the older generation cone sheets at the margin of the complex, but not in younger generation cone sheets. However, the mineralogical and isotopic data presented in this study clearly indicate that both deuteric and meteoric hydrothermal activity were spatially pervasive, affecting both marginal and central intrusions, and are likely to have prevailed at least until the emplacement of the youngest dated cone sheet at 7.3 Ma (Schirnack *et al.*, 1999).

A MODEL FOR THE HYDROTHERMAL EVOLUTION OF THE TEJEDA INTRUSIVE COMPLEX

The cone sheets and syenite stocks of the Miocene Tejeda Intrusive Complex (12.3–7.3 Ma) were emplaced at a shallow level (< 2 km) into the intra-caldera volcanic deposits of the Tejeda caldera, in response to recurrent replenishment of the underlying Fataga magma chamber system (Schirnack *et al.*, 1999) (Fig. 12). Cooling of the cone sheet magmas was accompanied by the expulsion of late magmatic, alkali-rich aqueous fluids, resulting in significant D- and H_2O -depletion in the parent magmas, and the crystallization of Na-bearing deuteric minerals (analcime, alkali-amphibole, and aegirine) at relatively high temperatures (~ 300 – 500°C). Almost continuous emplacement and degassing of the cone sheets over an ~ 5 Myr period resulted in the simultaneous formation of a zone of elevated temperatures in the surrounding volcanic deposits. This ‘heated zone’ promoted radial inflow of low $\delta^{18}\text{O}$ meteoric groundwaters, forming an area of hydrothermal circulation in the outer aureole of the cooling intrusive complex. Uplift (including resurgent doming) accompanying cone sheet and syenite emplacement resulted in increased tensile stress and associated fracturing at a shallow level directly above the intrusive complex (see Komuro, 1987). This near-surface fracture system, together with the main ring fault and peripheral fracture systems of the Tejeda caldera (e.g. Troll *et al.*, 2002), provided pathways for meteoric fluid entry and subsequent hydrothermal circulation. Upon solidification, the cone sheets and syenites were sufficiently cool to develop significant fracture permeability, allowing the surrounding meteoric–hydrothermal fluids to permeate the intrusive complex. Initial infiltration of these low $\delta^{18}\text{O}$ meteoric fluids at temperatures of ≥ 150 – 300°C was accompanied by the development of patchy to pervasive turbidity in alkali feldspar, and significant ^{18}O depletion in the rocks. Progressive infiltration of meteoric fluids into the cooling intrusive complex resulted in relatively minor low-temperature

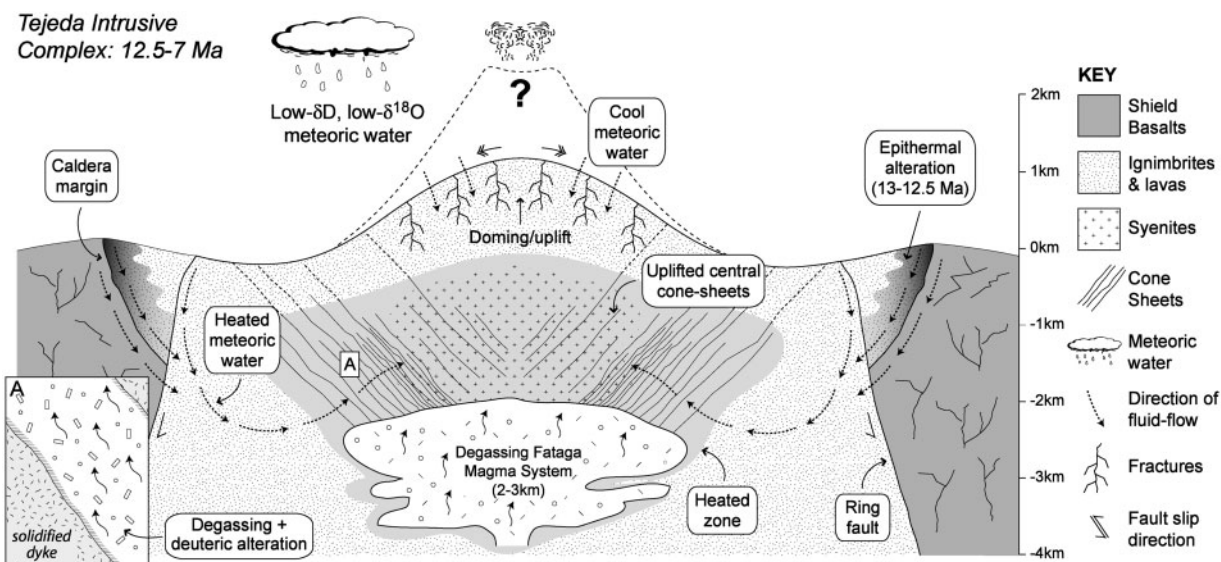


Fig. 12. Schematic diagram showing the evolution of the hydrothermal system associated with the Tejedá Intrusive Complex, and its spatial relationship to the Tejedá caldera. Emplacement and degassing of cone sheet magmas is accompanied by expulsion of late magmatic fluids, and the formation of interstitial deuterium phases (inset 'A' bottom left). Simultaneous formation of a 'heated zone' in the surrounding permeable volcanic deposits promotes radial inflow of shallow meteoric groundwaters. Progressive infiltration of heated meteoric fluids into the intrusive complex following solidification results in hydrothermal alteration of magmatic and deuterium mineral phases. Resurgent doming or uplift accompanying syenite emplacement allows for greater infiltration of cool, down-going meteoric waters (and enhanced retrograde alteration) at the centre of the intrusive complex. A large volcanic edifice, similar to that inferred to overlie the Fuerteventura basal complexes (Javoy *et al.*, 1986), may have existed above the Tejedá Intrusive Complex during the late Miocene, resulting in an increase in recharge altitude and a corresponding decrease in the $\delta^{18}\text{O}$ and δD values of local meteoric water.

alteration ($\leq 150^\circ\text{C}$) of magmatic and deuterium mineral phases to clay (chlorite–montmorillonite), decomposition of primary Fe–Ti oxides, and the precipitation of vein minerals (Mn-oxides, quartz), causing an overall increase in $\delta^{18}\text{O}$ values relative to 'normal' igneous compositions in some samples. Repeated intrusion of cone sheets with variable diameters over a period of ~ 5 Myr caused significant overprinting of isotopic values, and inhibited the formation of a systematic pattern of decreasing $\delta^{18}\text{O}$ from the centre to the margins of the intrusive complex. Resurgent doming associated with syenite emplacement promoted infiltration of cooler meteoric water at the centre of the intrusive complex, and enhanced retrograde alteration of more central cone sheets.

The Tejedá Intrusive Complex provides valuable insights into the sub-volcanic part of a large-scale caldera-hosted hydrothermal system, which persisted during the late Miocene (13–7 Ma) on Gran Canaria. In contrast to relatively short-lived or single-stage intrusions, which often record comparatively simple and systematic changes in mineralogical and isotopic composition, the hypabyssal rocks on Gran Canaria highlight the complex alteration textures and isotopic patterns produced in a relatively long-lived (~ 5 Myr), multi-intrusive system, reflecting progressively evolving hydrothermal conditions on a million-year timescale.

ACKNOWLEDGEMENTS

Robbie Goodhue (Trinity College Dublin) and Fayroza Rawoot (University of Cape Town) are thanked for their help during data acquisition. Assistance in the field from Alejandro Rodríguez González is greatly appreciated. The manuscript was improved by the thorough and insightful reviews of Luigi Dallai, Torsten Vennemann, John Wolff, and one anonymous reviewer. Early discussions with Carsten Schirnick, Hans-Ulrich Schmincke, and Paul van den Bogaard are also gratefully acknowledged.

FUNDING

Our work was made possible through financial support from the Irish Research Council for Science, Engineering, and Technology (IRCSET).

SUPPLEMENTARY DATA

Supplementary data for this paper are available at *Journal of Petrology* online.

REFERENCES

Abratis, M., Schmincke, H.-U. & Hansteen, T. (2002). Composition and evolution of submarine volcanic rocks from the central and

- western Canary Islands. *International Journal of Earth Sciences* **91**, 562–582.
- Agemar, T., Wörner, G. & Heumann, A. (1999). Stable isotopes and amphibole chemistry on hydrothermally altered granitoids in the North Chilean Precordillera: a limited role for meteoric water? *Contributions to Mineralogy and Petrology* **136**, 331–344.
- Ancochea, E., Huertas, M. J., Cantagrel, J. M., Coello, J., Fúster, J. M., Arnaud, N. & Ibarrola, E. (1999). Evolution of the Las Cañadas edifice and its implications for the origins of the Cañadas Caldera (Tenerife, Canary Islands). *Journal of Volcanology and Geothermal Research* **88**, 177–199.
- Bacon, C. H., Adami, J. H. & Lanphere, M. A. (1989). Direct evidence for the origin of low- ^{18}O silicic magmas: quenched samples of a magma chamber's partially-fused granitoid walls, Crater Lake, Oregon. *Earth and Planetary Science Letters* **96**, 199–208.
- Bindeman, I. N. & Valley, J. W. (2000). Formation of low- $\delta^{18}\text{O}$ rhyolites after caldera collapse at Yellowstone, Wyoming, USA. *Geology* **28**, 719–722.
- Bindeman, I. N., Ponomareva, V. V., Bailey, J. C. & Valley, J. W. (2004). Volcanic arc of Kamchatka: a province with high $\delta^{18}\text{O}$ magma sources and large-scale $^{18}\text{O}/^{16}\text{O}$ depletion of the upper crust. *Geochimica et Cosmochimica Acta* **68**, 841–865.
- Borthwick, J. & Harmon, R. S. (1982). A note regarding ClF_3 as an alternative to BrF_5 for oxygen isotope analysis. *Geochimica et Cosmochimica Acta* **46**, 1665–1668.
- Brandriss, M. E., Nelve, R. J., Bird, D. K. & O'Neil, J. R. (1995). Imprint of meteoric water on the stable isotope compositions of igneous and secondary minerals, Kap Edvard Holm complex, East Greenland. *Contributions to Mineralogy and Petrology* **121**, 74–86.
- Brandriss, M. E., Bird, D. K., O'Neil, J. R. & Cullers, R. L. (1996). Dehydration, partial melting, and assimilation of metabasaltic xenoliths in gabbros of the Kap Edvard Holm complex, East Greenland. *American Journal of Science* **296**, 333–393.
- Brown, P. R. L. & Ellis, A. J. (1970). The Ohaki–Broadlands hydrothermal area, New Zealand: mineralogy and related geochemistry. *American Journal of Science* **269**, 97–131.
- Burnham, C. W. (1997). Magmas and hydrothermal fluids. In: Barnes, H. L. (ed.) *Geochemistry of Hydrothermal Ore Deposits*, 3rd edn. New York: John Wiley, pp. 63–123.
- Burnham, C. W. & Ohmoto, H. (1980). Late-stage processes in felsic magmatism. *Mining Geology (Special Issue)* **8**, 1–11.
- Cabrera Santana, M. C., Pérez Torrado, F. J., Antón Gil, A. & Muñoz Sanz, F. (2006). *Volcanología de los Azulejos y su relación con las aguas subterráneas del Valle de La Aldea (Gran Canaria)*. Las Palmas de Gran Canaria: Cabildo de Gran Canaria, 153 p.
- Carracedo, J. C., Day, S., Guillou, H., Badiola, E. R., Canas, J. A. & Torrado, F. J. P. (1998). Hotspot volcanism close to a passive continental margin: The Canary Islands. *Geological Magazine* **135**, 591–604.
- Carracedo, J. C., Rodríguez Badiola, E., Guillou, H., Paterne, M., Scaillet, S., Pérez Torrado, F. J., Paris, R., Fra-Paleo, U. & Hansen, A. (2007). Eruptive and structural history of Teide volcano and rift zones of Tenerife, Canary Islands. *Geological Society of America Bulletin* **119**, 1027–1051.
- Chambers, L. M., Pringle, M. S. & Parish, R. R. (2005). Rapid formation of the Small Isles Tertiary centre constrained by precise $^{40}\text{Ar}/^{39}\text{Ar}$ and U–Pb ages. *Lithos* **79**, 367–384.
- Chao, G. Y. (1969). 20 (Cu) *Table for Common Minerals (Geological Paper 69-2)*. Ottawa, Ont.: Department of Geology, Carleton University.
- Cole, D. R., Larson, P. B., Riciputi, L. R. & Mora, C. L. (2004). Oxygen isotope zoning profiles in hydrothermally altered feldspars: Estimating the duration of water–rock interaction. *Geology* **32**, 29–32.
- Coplen, T. B. (1995). Reporting of stable hydrogen, carbon, and oxygen isotopic abundances. *Geothermics* **24**, 707–712.
- Coplen, T. B., Kendall, C. & Hopple, J. (1983). Comparison of stable isotope reference samples. *Nature* **302**, 236–238.
- Craig, H. (1961). Isotopic variations in meteoric waters. *Science* **133**, 1702–1703.
- Crisp, J. A. & Spera, F. J. (1987). Pyroclastic flows and lavas of the Mogán and Fataga formations, Tejedá volcano, Gran Canaria, Canary Islands: Mineral chemistry, intensive parameters and magma chamber evolution. *Contributions to Mineralogy and Petrology* **96**, 503–518.
- Criss, R. E. & Taylor, H. P., Jr (1983). A $^{18}\text{O}/^{16}\text{O}$ and D/H study of Tertiary hydrothermal systems in the southern half of the Idaho batholith. *Geological Society of America Bulletin* **94**, 640–663.
- Criss, R. E. & Taylor, H. P., Jr (1986). Meteoric hydrothermal systems. In: Valley, J. W., Taylor, H. P., Jr & O'Neil, J. R. (eds) *Stable Isotopes in High Temperature Geological Processes*. Mineralogical Society of America, *Reviews in Mineralogy* **16**, 373–424.
- Criss, R. E., Ekren, E. B. & Hardyman, R. F. (1984). Casto ring zone: A 4500-km² fossil hydrothermal system in the Challis Volcanic Field, central Idaho. *Geology* **12**, 331–334.
- Dansgaard, W. (1964). Stable isotopes in precipitation. *Tellus* **16**, 436–468.
- Deer, W. A., Howie, R. A. & Zussman, J. (1966). *An Introduction to the Rock-Forming Minerals*. Essex: Longman, 528 p.
- Donoghue, E., Troll, V. R., Harris, C., O'Halloran, A., Walter, T. R. & Pérez Torrado, F. J. (2008). Low-temperature hydrothermal alteration of intra-caldera tuffs, Miocene Tejedá caldera, Gran Canaria, Canary Islands. *Journal of Volcanology and Geothermal Research* **176**, 551–564.
- Edgar, A. D. & Parker, L. M. (1974). Comparison of melting relationships of some plutonic and volcanic peralkaline undersaturated rocks. *Lithos* **7**, 263–273.
- Eiler, J. M. (2001). Oxygen isotope variations of basaltic lavas and upper mantle rocks. In: Valley, J. W. & Cole, D. R. (eds) *Stable Isotope Geochemistry*. Mineralogical Society of America and Geochemical Society, *Reviews in Mineralogy and Geochemistry* **43**, 319–364.
- Elsenheimer, D. & Valley, J. W. (1993). Submillimeter scale zonation of $\delta^{18}\text{O}$ in quartz and feldspar, Isle of Skye, Scotland. *Geochimica et Cosmochimica Acta* **57**, 3669–3676.
- Farver, J. R. & Giletti, J. B. (1989). Patterns and processes of oxygen isotope exchange in a fossil meteoric hydrothermal system, Cuillins Gabbro Complex, Isle of Skye, Scotland. *Contributions to Mineralogy and Petrology* **102**, 24–33.
- Fehlhaber, K. & Bird, D. K. (1991). Oxygen-isotope exchange and mineral alteration in gabbros of the Lower Layered Series, Kap Edvard Hom Complex, East Greenland. *Geology* **19**, 819–822.
- Ferry, J. M. (1985a). Hydrothermal alteration of Tertiary igneous rocks from the Isle of Skye, northwest Scotland I. Gabbros. *Contributions to Mineralogy and Petrology* **91**, 264–282.
- Ferry, J. M. (1985b). Hydrothermal alteration of Tertiary igneous rocks from the Isle of Skye, northwest Scotland II. Granites. *Contributions to Mineralogy and Petrology* **91**, 283–304.
- Forester, R. W. & Taylor, H. P. (1976). ^{18}O -depleted igneous rocks from the Tertiary complex of the Isle of Mull, Scotland. *Earth and Planetary Science Letters* **32**, 11–17.
- Forester, R. W. & Taylor, H. P. (1977). $^{18}\text{O}/^{16}\text{O}$, D/H, and $^{13}\text{C}/^{12}\text{C}$ studies of the Tertiary igneous complex of Skye, Scotland. *American Journal of Science* **277**, 136–177.
- Friedman, I., Lipman, P. W., Obradovich, J. D. & Gleason, J. D. (1974). Meteoric water in magmas. *Science* **184**, 1069–1072.
- Gasparini, A., Custodio, E., Fontes, J.-C., Jimenez, J. & Nuñez, J. A. (1990). Exemple d'étude géochimique et isotopique de circulations

- aquíferes en terrain volcanique sous climat semi-aride (Amurga, Gran Canaria, Iles Canaries). *Journal of Hydrology* **114**, 61–91.
- Goble, R. J., Treves, S. B. & Ghazi, A. M. (1993). Comparison of the Rainy Ridge analcime phonolite sill and the Crowsnest volcanics, Alberta, Canada. *Canadian Journal of Earth Sciences* **30**, 1644–1649.
- Gonfiantini, R. (1973). *Isotope Study of Canary Islands Groundwater. Internal Report SPA/69/515*. Vienna: International Atomic Energy Agency (Isotope Hydrology Section), 21 p.
- Grunder, A. L. (1987). Low $\delta^{18}\text{O}$ silicic volcanic rocks at the Calabozos Caldera Complex, Southern Andes. *Contributions to Mineralogy and Petrology* **95**, 71–81.
- Gupta, A. K. & Fyfe, W. S. (1975). Leucite survival: The alteration to analcime. *Canadian Mineralogist* **13**, 361–363.
- Guthrie, G. D., Jr & Veblen, D. R. (1991). Turbid alkali feldspars from the Isle of Skye, northwest Scotland. *Contributions to Mineralogy and Petrology* **108**, 298–304.
- Hamilton, M. A., Pearson, D. G., Thompson, R. N., Kelley, S. P. & Emeleus, C. H. (1998). Rapid eruption of Skye lavas inferred from precise U–Pb and Ar–Ar dating of the Rum and Cuillin plutonic complexes. *Nature* **394**, 260–263.
- Harris, C. (1995). Oxygen isotope geochemistry of the Mesozoic anorogenic complexes of Damaland, northwest Namibia: evidence for crustal contamination and its effect on silica saturation. *Contributions to Mineralogy and Petrology* **122**, 308–321.
- Harris, C. & Erlank, A. J. (1992). The production of large-volume low- $\delta^{18}\text{O}$ rhyolites during the rifting of Africa and Antarctica: the Lebombo monocline, southern Africa. *Geochimica et Cosmochimica Acta* **56**, 3561–3570.
- Harris, C., Pronost, J. J. M., Ashwal, L. D. & Cawthorn, R. G. (2005). Oxygen and hydrogen isotope stratigraphy of the Rustenburg Layered Suite, Bushveld Complex: constraints on crustal contamination. *Journal of Petrology* **46**, 579–601.
- Harvey, P. K., Taylor, D. M., Hendrey, R. D. & Bancroft, F. (1973). An accurate fusion method for the analysis of rocks and chemically related materials by X-ray fluorescence spectrometry. *X-Ray Spectrometry* **2**, 33–44.
- Hernán, F. & Vélez, R. (1980). El sistema de diques conicos de Gran Canaria y la estimación estadística de sus características. *Estudios Geológicos* **36**, 65–73.
- Hildreth, W., Christiansen, R. L. & O’Neil, J. R. (1984). Catastrophic isotopic modification of rhyolitic magma at times of caldera subsidence, Yellowstone plateau volcanic field. *Journal of Geophysical Research* **89**, 8339–8369.
- Hoernle, K. & Schmincke, H.-U. (1993). The role of partial melting in the 15-Ma geochemical evolution of Gran Canaria—a blob model for the Canary hotspot. *Journal of Petrology* **34**, 599–626.
- Holloway, M. I., Bussy, F. & Vennemann, T. W. (2008). Low-pressure, water-assisted anatexis of basic dykes in a contact metamorphic aureole, Fuerteventura (Canary Islands): Oxygen isotope evidence for a meteoric fluid origin. *Contributions to Mineralogy and Petrology* **155**, 111–121.
- Horvath, L. & Gault, R. A. (1990). The mineralogy of Mont Saint-Hilaire, Quebec. *Mineralogical Record* **21**, 284–359.
- Javoy, M., Stillman, C. J. & Pineau, F. (1986). Oxygen and hydrogen isotope studies on the basal complexes of the Canary Islands: implications on the conditions of their genesis. *Contributions to Mineralogy and Petrology* **92**, 225–235.
- Karlsson, H. R. & Clayton, R. N. (1990). Oxygen isotope fractionation between analcime and water—an experimental study. *Geochimica et Cosmochimica Acta* **54**, 1359–1368.
- Kim, K.-T. & Burley, B. J. (1971). Phase equilibria in the system $\text{NaAlSi}_3\text{O}_8$ – NaAlSiO_4 – H_2O with special emphasis on the stability of analcime. *Canadian Journal of Earth Science* **8**, 311–337.
- Kogarko, L. N. & Romanchev, B. P. (1977). Temperature, pressure, redox conditions, and mineral equilibria in agpaitic nepheline syenites and apatite–nepheline rocks. *Geochemistry International* **14**, 113–128.
- Komuro, H. (1987). Experiments on cauldron formation: A polygonal cauldron and ring fractures. *Journal of Volcanology and Geothermal Research* **31**, 139–149.
- Larson, P. B. & Geist, D. J. (1995). On the origin of low- ^{18}O magmas: Evidence from the Casto pluton, Idaho. *Geology* **23**, 909–912.
- Larson, P. B. & Taylor, H. P., Jr (1986a). An oxygen-isotope study of water–rock interaction in the granite of Cataract Gulch, western San Juan Mountains, Colorado. *Geological Society of America Bulletin* **97**, 505–515.
- Larson, P. B. & Taylor, H. P., Jr (1986b). $^{18}\text{O}/^{16}\text{O}$ ratios in ash-flow tuffs and lavas erupted from the central Nevada caldera complex and the central San Juan caldera complex, Colorado. *Contributions to Mineralogy and Petrology* **92**, 146–156.
- Larson, P. B. & Taylor, H. P., Jr (1986c). An oxygen isotope study of hydrothermal alteration in the Lake City Caldera, San Juan Mountains, Colorado. *Journal of Volcanology and Geothermal Research* **30**, 47–82.
- Le Bas, M. J. (1971). Cone-sheets as a mechanism of uplift. *Geological Magazine* **108**, 373–376.
- Le Maitre, R. W., Bateman, O., Dudek, A., Keller, J., Lameyre, J., Le Bas, M. J., Sabine, P. A., Schmid, R., Sorensen, H., Streckeisen, A., Woolley, A. R. & Zanettin, B. (1989). *A Classification of Igneous Rocks and Glossary of Terms*. Oxford: Blackwell, 206 p.
- Lipman, P. W. & Friedman, I. (1975). Interaction of meteoric water with magma: an oxygen isotope study of ash-flow sheets from southern Nevada. *Geological Society of America Bulletin* **86**, 695–702.
- Luhr, J. F. & Gianetti, B. (1987). The brown leucitic tuff of Roccamonfina volcano (Roman Region, Italy). *Contributions to Mineralogy and Petrology* **95**, 420–436.
- Luhr, J. F. & Kyser, T. K. (1989). Primary igneous analcime: The Colima minettes. *American Mineralogist* **74**, 216–223.
- Lutz, T. M., Foland, K. A., Faul, H. & Srogi, L. A. (1988). The strontium and oxygen isotopic record of hydrothermal alteration of syenites from the Abu-Khruq complex, Egypt. *Contributions to Mineralogy and Petrology* **98**, 212–223.
- Markl, G. (2001). Stability of Na–Be minerals in late-magmatic fluids of the Ilímaussaq alkaline complex, South Greenland. *Geology of Greenland Survey Bulletin* **190**, 145–158.
- Markl, G. & Baumgartner, L. (2002). pH changes in peralkaline late-magmatic fluids. *Contributions to Mineralogy and Petrology* **144**, 331–346.
- Marks, M., Vennemann, T., Siebel, W. & Markl, G. (2003). Quantification of magmatic and hydrothermal processes in a peralkaline syenite–alkali granite complex based on textures, phase equilibria, and stable and radiogenic isotopes. *Journal of Petrology* **44**, 1247–1280.
- Marks, M., Vennemann, T., Siebel, W. & Markl, G. (2004). Nd-, O-, and H-isotopic evidence for complex, closed-system fluid evolution of the peralkaline Ilímaussaq intrusion, South Greenland. *Geochimica et Cosmochimica Acta* **68**, 3379–3395.
- Martí, J., Mitjavila, J. & Araña, V. (1994). Stratigraphy, structure and geochronology of the Las Cañadas caldera (Tenerife, Canary Islands). *Geological Magazine* **131**, 715–727.
- McBirney, A. I. (1993). *Igneous Petrology*. San Francisco, CA: Freeman, Cooper, 508 p.
- Muehlenbachs, K. (1986). Alteration of the oceanic crust and the ^{18}O history of seawater. In: Valley, J. W., Taylor, H. P., Jr & O’Neil, J. R. (eds) *Stable Isotopes in High Temperature Geological Processes*. Mineralogical Society of America, *Reviews in Mineralogy* **16**, 425–442.

- Muñoz Sanz, J. (1995). Estudio hidrogeológico del acuífero de La Aldea de San Nicolás, PhD thesis, Universidad de Las Palmas de Gran Canaria.
- Nabelek, P. I., O'Neil, J. R. & Papike, J. J. (1983). Vapour phase exsolution as a controlling factor in hydrogen isotope variation in granitic rocks: the Notch Peak granitic stock, Utah. *Earth and Planetary Science Letters* **66**, 137–150.
- Nelvé, R. J., Bandriss, M. E., Bird, D. K., MacWilliams, M. O. & O'Neil, J. R. (1994). Tertiary plutons monitor climate change in East Greenland. *Geology* **22**, 775–778.
- Niedermeier, D. R. D., Putnis, A., Geisler, T., Golla-Schindler, U. & Putnis, C. V. (2009). The mechanism of cation and oxygen isotope exchange in alkali feldspars under hydrothermal conditions. *Contributions to Mineralogy and Petrology* **157**, 65–76.
- Norrish, K. & Hutton, J. T. (1969). An accurate X-ray spectrographic method for the analysis of a wide range of geological samples. *Geochimica et Cosmochimica Acta* **33**, 431–453.
- O'Neil, J. R. & Taylor, H. P. (1967). The oxygen isotope and cation exchange chemistry of feldspars. *American Mineralogist* **52**, 1414–1437.
- Parsons, I. & Brown, W. L. (1984). Feldspars and the thermal history of igneous rocks. In: Brown, W. L. (ed.) *Feldspars and Feldspathoids*. Dordrecht: Reidel, pp. 317–371.
- Parsons, I., Mason, R. A., Becker, S. M. & Finch, A. A. (1991). Biotite equilibria and fluid circulation in the Klokken Intrusion. *Journal of Petrology* **32**, 1299–1333.
- Pearce, T. H. (1993). Analcime phenocrysts in igneous rocks: primary or secondary?—Discussion. *American Mineralogist* **78**, 225–259.
- Pérez Torrado, F. J., Cabrera Santana, M. C., Antón Gil, A. & Muñoz Sanz, F. (2004). Estratigrafía y petrología de los depósitos de 'Azulejos' del borde de la Caldera de Tejeda (Gran Canaria, Islas Canarias). *Geotemas* **6**, 159–162.
- Peters, T. J., Luth, W. C. & Tuttle, O. F. (1966). Melting of analcite solid solutions in system $\text{NaAlSi}_3\text{O}_8\text{-NaAlSi}_3\text{O}_8\text{-H}_2\text{O}$. *American Mineralogist* **51**, 736–753.
- Plümper, O. & Putnis, A. (2009). The complex hydrothermal history of granitic rocks: multiple feldspar replacement reactions under subsolidus conditions. *Journal of Petrology* **50**, 967–987.
- Post, J. E. (1999). Manganese oxide minerals: crystal structures and economic and environmental significance. *Proceedings of the National Academy of Sciences of the USA* **96**, 3447–3454.
- Putnis, A., Hinrichs, R., Putnis, C. V., Golla-Schindler, U. & Collins, L. G. (2007). Hematite in porous red-clouded feldspars: evidence for large-scale crustal fluid–rock interaction. *Lithos* **95**, 10–18.
- Rodríguez-Losada, J. A. & Martínez-Frías, J. (2004). The felsic complex of the Vallehermoso Caldera: interior of an ancient volcanic system (La Gomera, Canary Islands). *Journal of Volcanology and Geothermal Research* **137**, 261–284.
- Roux, J. & Hamilton, D. L. (1976). Primary igneous analcite—an experimental study. *Journal of Petrology* **17**, 244–257.
- Savin, S. M. & Epstein, S. (1970). Oxygen and hydrogen isotope geochemistry of clay minerals. *Geochimica et Cosmochimica Acta* **34**, 25–42.
- Scaillet, B. & Macdonald, R. (2001). Phase relations of peralkaline silicic magmas and petrogenetic implications. *Journal of Petrology* **42**, 825–845.
- Schiffman, P. & Staudigel, H. (1994). Hydrothermal alteration of a seamount complex on La Palma, Canary Islands: Implications for metamorphism in accreted terranes. *Geology* **22**, 151–154.
- Schiffman, P. & Staudigel, H. (1995). The smectite to chlorite transition in a fossil seamount hydrothermal system: The Basement Complex of La Palma, Canary Islands. *Journal of Metamorphic Geology* **13**, 487–498.
- Schirnick, C. (1996). Formation of an intracaldera cone sheet dike swarm (Tejeda caldera, Gran Canaria), PhD thesis, Christian-Albrechts-Universität, Kiel.
- Schirnick, C., van den Bogaard, P. & Schmincke, H.-U. (1999). Cone sheet formation and intrusive growth of an oceanic island—the Miocene Tejeda Complex on Gran Canaria (Canary Islands). *Geology* **27**, 207–210.
- Schmincke, H.-U. (1967). Cone sheet swarm, resurgence of Tejeda caldera, and the early geologic history of Gran Canaria. *Bulletin of Volcanology* **31**, 153–162.
- Schmincke, H.-U. (1976). The geology of the Canary Islands. In: Kunkel, G. (ed.) *Biogeography and Ecology in the Canary Islands*. The Hague: W. Junk, pp. 67–184.
- Schmincke, H.-U. (1982). Volcanic and chemical evolution of the Canary Islands. In: von Rad, U., Hinz, K., Sarnthein, M. & Seibold, E. (eds) *Geology of the Northwest African Continental Margin*. Berlin: Springer, pp. 273–306.
- Schmincke, H.-U. (1998). *Geological Field Guide of Gran Canaria (Parts 1 and 2)*. Witten: Pluto Press, 64 p.
- Schmincke, H.-U. & Swanson, D. A. (1966). Eine alte Caldera auf Gran Canaria. *Neues Jahrbuch für Geologische und Paläontologische Mitteilungen* **5**, 260–269.
- Schönenberger, J., Marks, M., Wagner, T. & Markl, G. (2006). Fluid–rock interaction in autoliths of agpaitic nepheline syenites in the Ilimaussaq intrusion, South Greenland. *Lithos* **91**, 331–351.
- Schroeder, B., Thompson, G., Sulanowska, M. & Ludden, J. N. (1980). Analysis of geologic materials using an automated X-ray fluorescence system. *X-Ray Spectrometry* **9**, 198–205.
- Sheppard, S. M. F. (1986a). Characterisation and isotopic variations in natural waters. In: Valley, J. W., Taylor, H. P., Jr & O'Neil, J. R. (eds) *Stable Isotopes in High Temperature Geological Processes. Mineralogical Society of America, Reviews in Mineralogy* **16**, 165–183.
- Sheppard, S. M. F. (1986b). Igneous rocks: III. isotopic case studies of magmatism in Africa, Eurasia and oceanic islands. In: Valley, J. W., Taylor, H. P., Jr & O'Neil, J. R. (eds) *Stable Isotopes in High Temperature Geological Processes. Mineralogical Society of America, Reviews in Mineralogy* **16**, 319–371.
- Sheppard, S. M. F. & Gilg, H. A. (1996). Stable isotope geochemistry of clay minerals: the story of sloppy, sticky, lumpy and tough. *Clay Minerals* **31**, 1–24.
- Sumita, M. & Schmincke, H.-U. (1998). Tephra event stratigraphy and emplacement of volcanoclastic sediments, Mogán and Fataga stratigraphic intervals, Part I: Mineral and chemical stratigraphy of volcanoclastic units and correlation to the sub-aerial record. In: Weaver, P. P. E., Schmincke, H.-U., Firth, J. V. & Duffield, W. (eds) *Proceeding of the Ocean Drilling Program, Scientific Results, 157*. College Station, TX: Ocean Drilling Program, pp. 219–264.
- Taylor, B. E. (1986). Magmatic volatiles: isotopic variation of C, H, and S. In: Valley, J. W., Taylor, H. P., Jr & O'Neil, J. R. (eds) *Stable Isotopes in High Temperature Geological Processes. Mineralogical Society of America, Reviews in Mineralogy* **16**, 185–225.
- Taylor, B. E., Eichelberger, J. C. & Westrich, H. R. (1983). Hydrogen isotopic evidence of rhyolitic magma degassing during shallow intrusion and eruption. *Nature* **306**, 541–545.
- Taylor, H. P., Jr (1968). The oxygen isotope geochemistry of igneous rocks. *Contributions to Mineralogy and Petrology* **19**, 1–71.
- Taylor, H. P., Jr (1974). The application of oxygen and hydrogen isotope studies to problems of hydrothermal alteration and ore deposition. *Economic Geology* **69**, 843–883.
- Taylor, H. P., Jr (1977). Water/rock interactions and the origin of H_2O in granitic batholiths. *Journal of the Geological Society, London* **133**, 509–558.

- Taylor, H. P., Jr (1997). Oxygen and hydrogen isotope relationships in hydrothermal mineral deposits. In: Barnes, H. L. (ed.) *Geochemistry of Hydrothermal Ore Deposits*, 3rd edn. New York: John Wiley, pp. 229–302.
- Taylor, H. P., Jr & Epstein, S. (1963). $^{18}\text{O}/^{16}\text{O}$ ratios in rocks and coexisting minerals of the Skaargaard intrusion. *Journal of Petrology* **4**, 51–74.
- Taylor, H. P., Jr & Forester, R. W. (1970). Low $\delta^{18}\text{O}$ igneous rocks from the intrusive complexes of Skye, Mull, and Ardnamurchan, western Scotland. *Journal of Petrology* **12**, 465–497.
- Taylor, H. P., Jr & Sheppard, S. M. F. (1986). Igneous rocks: I. Processes of isotopic fractionation and isotope systematics. In: Valley, J. W., Taylor, H. P., Jr & O'Neil, J. R. (eds) *Stable Isotopes in High Temperature Geological Processes*. Mineralogical Society of America, *Reviews in Mineralogy* **16**, 227–271.
- Thompson, A. J. B. & Thompson, J. F. H. (1996). *Atlas of Alteration: A Field and Petrological Guide to Hydrothermal Alteration Minerals*. Newfoundland: Geological Association of Canada—Mineral Deposits Division, 119 p.
- Troll, V. R. & Schmincke, H.-U. (2002). Alkali-feldspar in compositionally zoned peralkaline rhyolite/trachyte ignimbrite 'A', Gran Canaria: implications for magma mixing and crustal recycling. *Journal of Petrology* **43**, 243–270.
- Troll, V. R., Walter, T. R. & Schmincke, H.-U. (2002). Cyclic caldera collapse: piston or piecemeal subsidence? Field and experimental evidence. *Geology* **30**, 135–138.
- Troll, V. R., Nicoll, G. R., Donaldson, C. H. & Emeleus, H. C. (2008). Dating the onset of volcanism at the Rum Igneous Centre, NW Scotland. *Journal of the Geological Society, London* **165**, 651–659.
- van den Bogaard, P. & Schmincke, H.-U. (1998). Chronostratigraphy of Gran Canaria. In: Weaver, P. P. E., Schmincke, H.-U., Firth, J. V. & Duffield, W. (eds) *Proceedings of the Ocean Drilling Program, Scientific Results, 157*. College Station, TX: Ocean Drilling Program, pp. 127–140.
- Vennemann, T. W. & O'Neil, J. R. (1993). A simple and inexpensive method of hydrogen isotope and water analyses of minerals and rocks based on zinc reagent. *Chemical Geology* **103**, 227–234.
- Vennemann, T. W. & Smith, H. S. (1990). The rate and temperature of reaction of ClF_3 with silicate minerals, and their relevance to oxygen isotope analysis. *Chemical Geology* **86**, 83–88.
- Walker, F. D. L., Lee, M. R. & Parsons, I. (1995). Micropores and micropore texture in alkali-feldspars—geochemical and geophysical implications. *Mineralogical Magazine* **59**, 505–534.
- Wenner, D. B. & Taylor, H. P. (1971). Temperatures of serpentinization of ultramafic rocks based on $^{18}\text{O}/^{16}\text{O}$ fractionation between coexisting serpentine and magnetite. *Contributions to Mineralogy and Petrology* **32**, 165–185.
- White, N. C. & Hedenquist, J. W. (1990). Epithermal environments and styles of alteration: variations and their causes, and guidelines for exploration. *Journal of Geochemical Exploration* **36**, 445–474.
- Wilkinson, J. F. G. (1968). Analcimes from some potassic igneous rocks and aspects of analcime-rich igneous assemblages. *Contributions to Mineralogy and Petrology* **18**, 252–269.
- Wilkinson, J. F. G. & Hensel, H. D. (1994). Nephelines and analcimes in some alkaline igneous rocks. *Contributions to Mineralogy and Petrology* **118**, 79–91.
- Witt-Eickschen, G., Evangelakakis, C., Seck, H. A., Kroll, H. & Gurbanov, A. G. (1996). Ordering and exsolution processes in Or-rich alkali-feldspar megacrysts from the Eldzhurtinskiy granite (Caucasus). *Contributions to Mineralogy and Petrology* **124**, 71–81.
- Wolff, J. A. (1987). Crystallisation of nepheline syenite in a subvolcanic magma system: Tenerife, Canary Islands. *Lithos* **20**, 207–223.
- Wolff, J. A. & Toney, J. B. (1993). Trapped liquid from a nepheline syenite: a re-evaluation of Na-, Zr-, F-rich interstitial glass in a xenolith from Tenerife, Canary Islands. *Lithos* **29**, 285–293.
- Wolff, J. A., Grandy, J. S. & Larson, P. B. (2000). Interaction of mantle-derived magma with island crust? Trace element and oxygen isotope data from the Diego Hernandez Formation, Las Cañadas, Tenerife. *Journal of Volcanology and Geothermal Research* **103**, 343–366.
- Worden, R. H., Walker, F. D. L., Parsons, I. & Brown, W. L. (1990). Development of microporosity, diffusion channels and deuteric coarsening in perthitic alkali feldspars. *Contributions to Mineralogy and Petrology* **104**, 507–515.
- Yeh, H. W. (1980). D/H ratios and late-stage dehydration of shales during burial. *Geochimica et Cosmochimica Acta* **44**, 341–352.